

UCSF

UC San Francisco Previously Published Works

Title

The fate of intracellular S1P regulates lipid droplet turnover and lipotoxicity in pancreatic beta-cells.

Permalink

<https://escholarship.org/uc/item/2wk8j2w3>

Journal

Journal of Lipid Research, 65(8)

Authors

Tang, Yadi

Majewska, Mariola

Leß, Britta

[et al.](#)

Publication Date

2024-08-01

DOI

10.1016/j.jlr.2024.100587

Copyright Information

This work is made available under the terms of a Creative Commons Attribution License, available at <https://creativecommons.org/licenses/by/4.0/>

Peer reviewed



The fate of intracellular S1P regulates lipid droplet turnover and lipotoxicity in pancreatic beta-cells

Yadi Tang¹, Mariola Majewska¹, Britta Leß¹, Ilir Mehmeti¹, Philipp Wollnitzke², Nina Semleit², Bodo Levkau², Julie D. Saba³, Gerhild van Echten-Deckert⁴, and Ewa Gurgul-Convey^{1*}

¹Institute of Clinical Biochemistry, Hannover Medical School, Hannover, Germany; ²Institute of Molecular Medicine III, University Hospital Düsseldorf and Heinrich Heine University, Düsseldorf, Germany; ³Division of Hematology/Oncology, Department of Pediatrics, University of California, San Francisco, Oakland, CA, USA; and ⁴Life & Medical Sciences Institute, University Bonn, Bonn, Germany

Abstract Lipotoxicity has been considered the main cause of pancreatic beta-cell failure during type 2 diabetes development. Lipid droplets (LD) are believed to regulate the beta-cell sensitivity to free fatty acids (FFA), but the underlying molecular mechanisms are largely unclear. Accumulating evidence points, however, to an important role of intracellular sphingosine-1-phosphate (SIP) metabolism in lipotoxicity-mediated disturbances of beta-cell function. In the present study, we compared the effects of an increased irreversible SIP degradation (SIP-lyase, SPL overexpression) with those associated with an enhanced SIP recycling (overexpression of SIP phosphatase 1, SGPP1) on LD formation and lipotoxicity in rat INSIE beta-cells. Interestingly, although both approaches led to a reduced SIP concentration, they had opposite effects on the susceptibility to FFA. Overexpression of SGPP1 prevented FFA-mediated caspase-3 activation by a mechanism involving an enhanced lipid storage capacity and prevention of oxidative stress. In contrast, SPL overexpression limited LD biogenesis, content, and size, while accelerating lipophagy. This was associated with FFA-induced hydrogen peroxide formation, mitochondrial fragmentation, and dysfunction, as well as ER stress. These changes coincided with the upregulation of proapoptotic ceramides but were independent of lipid peroxidation rate. Also in human EndoC-βH1 beta-cells, suppression of SPL with simultaneous overexpression of SGPP1 led to a similar and even more pronounced LD phenotype as that in INSIE-SGPP1 cells. Thus, intracellular SIP turnover significantly regulates LD content and size and influences beta-cell sensitivity to FFA.

Supplementary key words diabetes • beta-cells • lipid droplets • free fatty acids • insulin-secreting cells • sphingosine-1 phosphate • ceramide • mitochondria

Type 2 diabetes mellitus (T2DM) is a major metabolic disorder affecting millions of people worldwide (1). In

addition to hyperglycemia caused by the dysfunction of pancreatic beta-cells that secrete insulin and to insulin resistance of metabolic tissues, the disease is associated with chronic hyperlipidemia (1). Chronic exposure of pancreatic beta-cells to free fatty acids (FFA) is believed to play a crucial role in the activation of integrated stress response, eventually leading to beta-cell dysfunction and death (2–6). Lipotoxicity in beta-cells has been associated with *i*) oxidative stress, *ii*) endoplasmic reticulum (ER) and mitochondrial disturbances, *iii*) dysregulation of autophagy, *iv*) biosynthesis of complex lipid species [e.g., sphingolipids such as ceramide and sphingosine-1-phosphate (SIP)], and *v*) decreased lipid storage capacity (2, 3). The effects of various FFA differ substantially, depending on their chemical structure and metabolic pathways induced at various subcellular sites (5–7). Interestingly, *in vitro* experiments using beta-cell lines strongly indicate that monounsaturated fatty acids such as oleate (OA), which are protective in rodent beta-cells (2, 8, 9), are toxic to human beta-cells (5, 8, 10, 11); however, the underlying mechanisms remain unclear. Moreover, the sensitivity to FFA of isolated human islets is characterized by heterogeneity, similarly to a profound variability of disease progression and severity in T2DM patients.

Interestingly, recent studies indicate that SIP might be a crucial element in this context. An elevated plasma concentration of SIP has been shown to coincide with insulin resistance, obesity, and hyperinsulinemia (12–14). SIP belongs to a complex family of sphingolipids, which are biosynthesized mainly from palmitate (PA) and L-serine (condensation of palmitoyl-CoA with Ser in the ER). Additionally, use of other FFA (e.g., OA) and amino acids, though with a lower efficiency and particularly upon a PA shortage (15), has been reported resulting in the generation of atypical sphingolipids, which represent approximately 15% of sphingolipids in

*For correspondence: Ewa Gurgul-Convey, Gurgul-Convey.Ewa@mh-hannover.de.

human plasma (16). In vitro incubations with SIP have been shown to potentiate glucose-induced insulin secretion and to stimulate beta-cell proliferation (17, 18), which was associated with elevated cAMP generation mediated by the stimulation of SIP receptors on beta-cells. The specific effects of intracellular SIP are influenced by the subcellular localization of its biosynthesis (19–22). SIP can be generated from sphingosine by the action of two isoenzymes, sphingosine kinase 1 (SK1), active primarily at the plasma membrane, and sphingosine kinase 2 (SK2), localized to the ER, mitochondria, and nucleus (23). Of note, pancreatic beta-cells express predominantly SK2 (24). Intriguingly, the two SKs appear to have opposite effects on the toxicity of PA, the most abundant saturated fatty acid in human serum. Thus, SK2 knockdown was reported to protect beta-cells against PA toxicity (21, 22), while similar results were obtained in SK1 overexpressing cells (19). Once generated, SIP can undergo two fates leading to its decreased concentration: *i*) dephosphorylation (recycling) by SIP phosphatases 1 or 2 (SGPPI or 2) back to sphingosine or *ii*) irreversible cleavage by SIP lyase (SPL) into ethanolamine phosphate and hexadecenal (25, 26). The SGPP-derived sphingosine can be re-phosphorylated to SIP or used as a substrate for ceramide generation by ceramide synthases (25). Elevated intracellular ceramide formation has been shown to mediate PA toxicity in beta-cells (19, 27–30). Note that beta-cells express predominantly SGPP2 (17), which has been shown to play an important role in apoptosis in other cell types (31). In contrast, SGPPI, which is related to antiapoptotic effects in other tissues, is very weakly expressed in beta-cells (17). To our knowledge, no data regarding the role of SGPPI in lipotoxicity in beta-cells have been published so far. The observations made in a SGPP2 KO mouse model indicate that SGPP2 is involved in beta-cell proliferation and ER function (32). The SIP-degrading enzyme SPL is expressed in a low/medium range in rodent beta-cells, while being abundantly expressed in human beta-cells (8, 17). Recently, we have shown that SPL may be crucially involved in the lipotoxic beta-cell death, an observation that coincided with a decreased number of lipid droplets (LD) in response to OA (8). Indeed, sphingolipids have been shown to regulate LD biogenesis in various cell types (33, 34), though the role of SIP turnover in this context remains unclear (33, 34).

LDs are fat storage organelles that are formed in the ER and are composed of a neutral lipid hydrophobic core and an external phospholipid monolayer containing specific proteins, such as Plin 1–5 (perilipins 1–5) (35, 36). LDs are hubs of cellular lipid and energy metabolism, and their contact with other cell organelles, such as mitochondria or lysosomes is crucial for lipid transfer and cell metabolism (35). The biogenesis of LDs continues unabated when ER function is well maintained, and it is regulated by the intracellular content of specific lipids, including neutral lipids and

ceramides, particularly in the acylated form (37), by the activity of enzymatic lipid metabolism machinery (such as Dgat2) and by a proper expression of various LD-associated proteins, such as seipin or Plin 1–5 (36). The mechanism of LD turnover depends on their size and is regulated by lipophagy and lipolysis (38). LDs modulate cell fate, ER stress, and mitochondrial dysfunction by isolating lipids and inhibiting lipotoxicity (33, 34).

The role of LDs in beta-cells still remains rather unclear. In some studies, LD formation was correlated with OA-mediated protection against PA toxicity in rodent beta-cells, while others failed to observe such a link (7, 9, 39). Enhanced incorporation of PA into LDs has been recently proposed as a mechanism of the stearoyl-CoA desaturase 1 (SCD1)-mediated protection of beta-cells (40).

In the present study, we used two approaches to influence SIP metabolism: *i*) overexpression of SGPPI and *ii*) overexpression/suppression of SPL. This strategy enabled us to discern whether a decreased concentration of SIP as such regulates the sensitivity of beta-cells to FFA or if additional aspects including the compartmentalization and activation of specific metabolic pathways in response to upregulation of each of these two enzymes are key regulatory mechanisms in LD turnover and lipotoxic beta-cell damage. We show that reduction of SIP by directing its metabolism towards recycling or cleavage indeed causes profound perturbations of LD turnover yet by different molecular mechanisms resulting in distinct sensitivity to FFA-mediated toxicity.

MATERIALS AND METHODS

Cell culture and FFA incubations

Rat insulin-secreting INSIE cells (a kind gift of Prof. C. Wollheim, Geneva, Switzerland) were cultured in humidified atmosphere at 37°C and 5% CO₂. The cell lines used were routinely checked for mycoplasma and were free from mycoplasma contamination. INSIE cells were cultured in RPMI 1640 medium supplemented with 10 mM glucose, 10% fetal calf serum, penicillin and streptomycin, 10 mM HEPES (Serva, Heidelberg, Germany), 2 mM glutamine, 1 mM sodium-pyruvate (Sigma-Aldrich, Taufkirchen, Germany), and 50 µM of 2-mercaptoethanol (8, 17). EndoC-βHI beta-cells were cultured onto coated dishes or plates (fibronectin and ECM) in a DMEM 31885029 cell culture medium (5.5 mM glucose) without serum but supplemented with 2% BSA, penicillin and streptomycin, 10 µM nicotinamide, 2.5 µg/ml transferrin, 6.7 ng/ml sodium selenite, and 50 µM of 2-mercaptoethanol as described earlier (8). For testing, cells were washed with PBS, followed by incubation with FFA (palmitate or oleate, Merck) at the concentration of 500 µM for 24 h in cell culture media with 1% fetal calf serum and FFA-free BSA as described earlier (8). The stock solutions of PA and OA (50 mM) were freshly prepared using 90% ethanol as a solvent at 62° (8). The ratio between FFA and added BSA was equivalent to a FFA/BSA molar ratio of 3.3 for INS-IE or 5 for EndoC-βHI cells, representing the FFA/BSA ratios under pathological conditions (41). The calculated free, unbound FFA fraction represent approximately three- to five-

times the concentration of unbound FFAs measured in the plasma of healthy lean individuals (42, 43). These calculated concentrations of free, unbound PA may correlate with the three-fold elevated concentrations of FFAs observed in individuals diagnosed with T2DM (44).

Modification of the expression levels of SPL and SGPP1

The human SPL was stably overexpressed in insulin-secreting INSIE cells as described earlier (17). The human SGPP1 was overexpressed by a lentiviral transduction protocol using the pCLV-Ubic-MCS-IRES-SGPP1 (Sirion Biotech). Positive clones were selected using antibiotics (G418 for SPL, puromycin for SGPP1), and the gene and protein expression levels of SPL and SGPP1 were confirmed. Transfections with empty vectors did not affect INSIE cell viability or susceptibility to FFA (data not shown). For INSIE-ctr cells, we refer to the pooled data from untransfected (no selective antibiotic), pcDNA3-empty (mock, G418), and pCLV-Ubic-MCS-IRES-empty (mock, puromycin)-transfected INSIE cells. Our group recently published observations on the role of SPL in lipotoxicity in beta-cells (8). In the present study, we used for comparison the same cell clone as we described previously (8). However, these cells were generated using a SPL-GFP fusion construct, which results in a bright green fluorescence signal with SPL overexpression. Thus, for all experiments requiring fluorescence measurements of other parameters, we used cells transfected with an SPL construct lacking tagged GFP. Control experiments have shown that transfections with either the SPL-GFP or the SPL-without GFP constructs result in successful overexpression (C_T of 20–23 in real-time qRT-PCR) of the active enzyme at the similar level [(8) and Fig. 1]. EndoC- β HI-ctr and SGPP1-overexpressing human beta-cells were transiently transfected with validated Silencer[®]Select RNAi against human SPL (80 nM, assay SI6965, Thermo Fisher Scientific) or a scramble siRNA (siQ, Ambion[™]Silencer Negative Control, Thermo Fisher Scientific) using Lipofectamine RNAiMax in OptiMEM medium according to the protocol (8). Twenty-four hours after transfection cell culture medium was changed. Seventy-two hours post-transfection, FFA incubations were started as described above.

Viability, caspase-3/7, and ATP assay

INSIE cells were seeded onto 96-well plates at a concentration of 30,000 cells/well and cultured for 48 h. Thereafter, cells were treated with FFAs for 24 h, and cell viability was determined by a microplate-based MTT assay [3-(4,5-dimethylthiazol-2-yl)-2,5-diphenyl tetrazolium bromide (Serva, Heidelberg, Germany)] as previously described (8, 17). The MTT assay is based on the conversion of MTT into formazan crystals by living cells and detects total mitochondrial activity, which correlates with the number of cells. In EndoC- β HI-ctr and SGPP1-overexpressing beta-cells, the sensitivity to FFA-induced apoptosis after knock-out of SPL was measured 24 h after FFAs incubation by a 96-well-based chemiluminescence Caspase-3/7-Glo assay (Promega) according to the manufacturer's protocol. ATP content was measured after exposure to FFA by ATPLite assay, according to the manufacturer's protocol (17).

Oxidative stress assessment

To detect overall oxidative and nitrosative stress, INSIE cells were seeded onto 96-well black plates. Before addition of

FFA, cells were pre-incubated with 10 μ M dichlorodihydrofluorescein diacetate DCFDA- H_2 (Thermo Fisher Scientific, Bremen, Germany) for 40 min at 37°C. Plates were analyzed at 480/520 nm excitation/emission using the fluorescence reader Synergy Mx multi-mode microplate reader (BioTek, Winooski, VT) as described earlier (8, 17). Each condition was analyzed at least in duplicate. Data were normalized to cell viability and expressed as a % of untreated cells. The subcellular hydrogen peroxide (H_2O_2) generation was estimated using fluorescence sensor HyPer proteins. Cells expressing HyPer proteins in cytoplasm (Hyper-Cyto), mitochondria (Hyper-Mito), or peroxisomes (Hyper-Peroxi) were seeded onto Mat-Tek glass bottom 35 mm dish (MatTek Corporation, Ashland). Cells were cultured for 48 h and afterwards exposed to FFAs for 24 h. Live cell imaging was performed using a CFP-YFP dual filter (excitation, 427 nm and 504 nm; emission, 520 nm) with a Olympus IX 81 inverted microscope system and the CellSens software (Olympus, Hamburg, Germany) for imaging and analysis. Shown are representative pictures from $n = 3$ individual experiments.

RNA isolation, cDNA synthesis, and real-time RT-PCR

Total RNA from insulin secreting INSIE cell clones was obtained using the RNeasy kit (Qiagen, Hilden, Germany). The quality of the total RNA was verified by agarose gel electrophoresis. RNA was quantified spectrophotometrically at 260/280 nm. Thereafter, 2 μ g of RNA were reverse transcribed into cDNA using a random hexamer primer (Life Technologies) and RevertAid H Minus M-MuLV reverse transcriptase (Thermo Fisher Scientific, Bremen, Germany). QuantiTect SYBR Green[™] technology (Qiagen), which uses a fluorescent dye that binds only double-stranded DNA, was employed. The reactions were performed on a ViiA7 real-time PCR system (Life Technologies) with the following protocol: 50°C for 2 min, 95°C for 10 min, and 40 cycles comprising a melting step at 95°C for 15 s, an annealing step at 62°C for 60 s, and an extension step at 72°C for 30 s. The quality of reactions was controlled by the analysis of melting curves. Each sample was amplified as triplicate. Data normalization was performed against the geometric mean of the housekeeping gene β -actin. The primer sequences are given in [supplemental Table S1](#).

Western blot analyses

Cells were homogenized in ice-cold PBS containing protease inhibitors (Roche, Mannheim, Germany) using short bursts (Braun-Sonic 125 Homogenizer, Quigley-Rochester, Rochester, NY). Protein content was determined by the BCA assay (Pierce). For Western blotting, 20–40 μ g of total protein was resolved by SDS-PAGE and then electroblotted onto membranes. Immunodetection was performed using specific primary antibodies ([supplemental Table S2](#)) as described (8). Pictures were captured by the INTAS chemiluminescence detection system (Intas Science Imaging Instruments, Göttingen, Germany). The intensity of bands was quantified through densitometry with Gel-Pro Analyzer version 4.0 software (Media Cybernetics, Silver Spring, MD).

Immunofluorescence staining

For immunofluorescence staining, INSIE cells were seeded onto collagen-coated glass slides and incubated as described above. The immunofluorescence staining and detection was

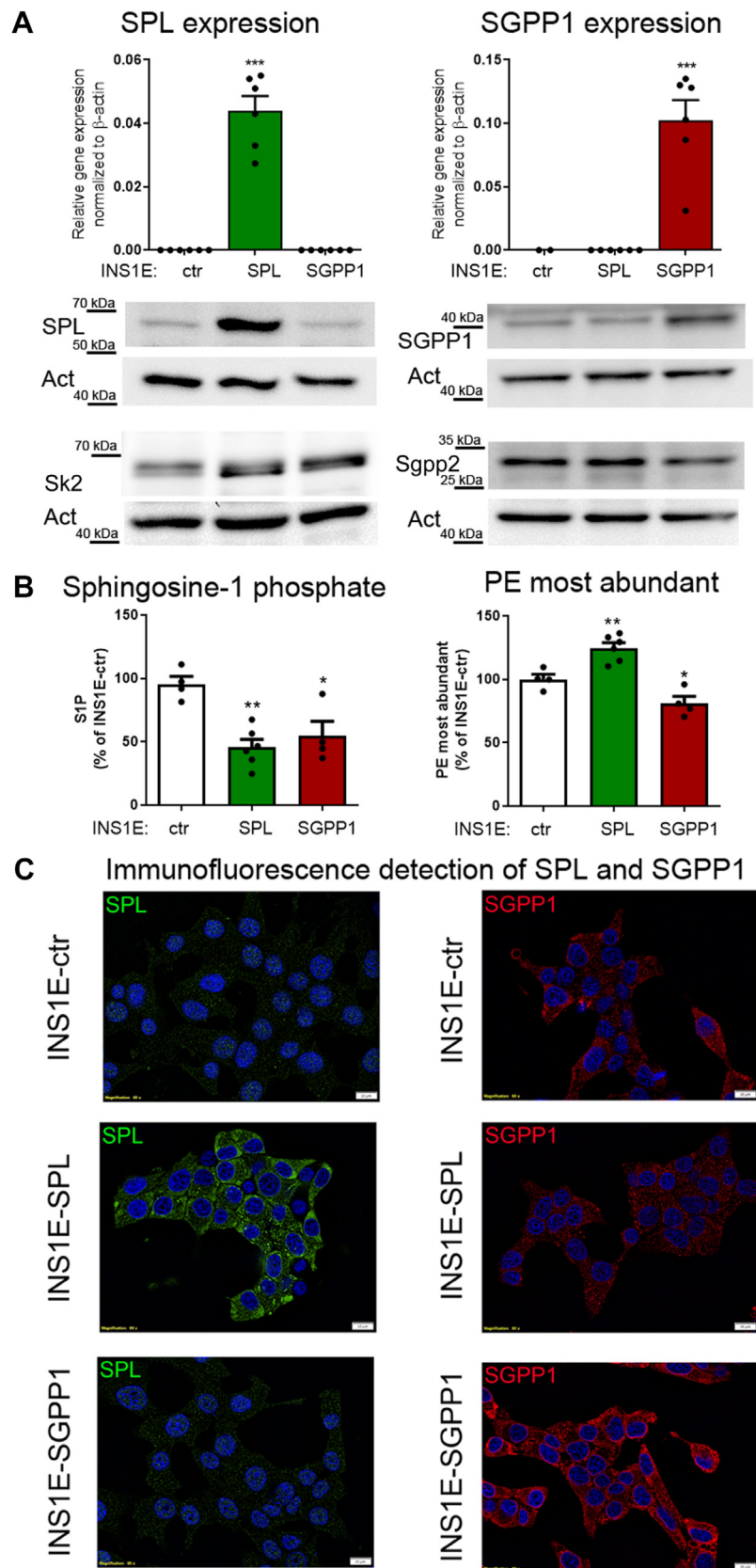


Fig. 1. Overexpression of human SPL and human SGPP1 in insulin-secreting INSIE cells. Shown are (A) gene and protein expression of human SPL and human SGPP1 measured by qRT-PCR and Western blotting, (B) SIP concentration measured by ELISA and content of the most abundant PE (phosphatidylethanolamine, PE 34:1, 36:1, 36:2, and 38:4) measured by mass-spec; changes in SIP and PE content are shown as % of concentrations in INSIE-ctr cells, $n = 4$. (C) representative immunofluorescence pictures (from $n = 2$) after staining with antibodies for the detection of rat and human SPL and SGPP1 (*green*-SPL, *red*-SGPP1; note that since both primary antibodies were

performed as described before (45). For SPL and SGPP1 detection, slides ($n = 2$) were incubated with primary antibodies (rabbit polyclonal anti-SPL (Santa Cruz) or rabbit polyclonal anti-SGPP1 (Thermo Fisher Scientific)), followed by secondary antibodies (anti-rabbit Alexa Fluor 488-conjugated IgG or anti-rabbit Alexa Fluor 647-conjugated IgG, both from Dianova, Hamburg). For a parallel detection of mitochondrial network changes and ceramide ($n = 3$), cells were incubated with the 250 nM Mitotracker-Red™ (Thermo Fisher Scientific, Bremen, Germany) in Krebs-Ringer buffer for 10 min at 37°C, following washing with PBS and an overnight fixation with 4% (w/v) paraformaldehyde in PBS (slides were kept in dark) (45). After fixation, cells were washed three times with PBS for 5 min. After a 20 min blocking in PBS with 0.1% Triton X-100 and 1% (v/v) BSA at room temperature (20°C), slides were washed again as above. The slides were incubated overnight at 4°C with mouse anti-Ceramide antibody (1:50 dilution from Biozol, Eching, Germany) and then washed three times with PBS. The cells were incubated with secondary antibodies for 1 h [Alexa Fluor 488-conjugated anti-mouse IgG, 1:200 dilution (Dianova, Hamburg, Germany)]. For nuclear counterstaining, 300 nM 4,6-diamidino-2-phenylindole (DAPI) was used for 5 min at room temperature. Slides were thereafter mounted with Mowiol (Merck, Darmstadt, Germany) plus 0.6% Dabco (Sigma Aldrich, Munich, Germany). Images were captured and analyzed using the CellSens software (Olympus, Hamburg, Germany) on the Olympus IX81 inverted microscope system.

Analysis of LD content and size

Cells were seeded onto 6-well plates and incubated as described above. Cells were trypsinized and fixed in 1% paraformaldehyde for 15 min at room temperature. Thereafter, cells were stained with Oil Red O solution (Sigma-Aldrich, Munich, Germany) followed by DAPI staining and washed twice with PBS (8). LD formation was analyzed using the CellSens/Olympus IX81 inverted microscope system (40× objective, Olympus, Hamburg, Germany) ($n = 4$ –6 independent experiments). The area within the INSIE cell clones was quantified by the use of CellSens Software (Olympus, Hamburg, Germany) at 546 nm excitation and 580 nm emission. For each condition, five to seven randomly selected images (each containing 3 to 10 cells) were used to quantify the proportion of the LD area to the total cell area with the phase analysis module of the CellSens software. Additionally, the size of LDs was estimated by the measurements of cell perimeter and grouping cells into three categories (small, medium, and large). The mean number of small, medium, and large LDs per cell was calculated for each condition and presented as % of total number of LDs of all sizes.

Visualization of neutral lipids and lipophagy

INSIE cells were seeded onto collagen-coated glass slides and incubated as described above. For a parallel detection of lysosomes and neutral lipids, cells were loaded with 250 nM LysoTracker™ Deep Red (Thermo Fisher Scientific, Waltham, Bremen, Germany) in Krebs-Ringer buffer for 10 min at 37°C, following washing with PBS and fixation with 4% (w/v) paraformaldehyde in PBS for 30 min at room temperature

(slides were kept in dark). After fixation, cells were rinsed with PBS three times. After washing, cells were incubated with IX HCS LipidTOX™ green neutral lipid stain (1:1,000 dilution, Thermo Fisher Scientific, Waltham, MA) at room temperature for 30 min. For nuclear counterstaining, 300 nM DAPI was used for 5 min at room temperature. Slides were thereafter mounted with Mowiol (Merck, Darmstadt, Germany) plus 0.6% Dabco (Sigma-Aldrich, Munich, Germany). Images were captured and analyzed using the CellSens software (Olympus, Hamburg, Germany) on the Olympus IX81 inverted microscope system. Shown are representative pictures of $n = 3$ individual experiments.

Measurement of SIP

Samples were prepared using lysis buffer: 20 mM PIPES, 150 mM NaCl, 1 mM EGTA, 1% (v/v) Triton X-100, 1.5 mM MgCl₂, 0.1% SDS, 1 mM sodium orthovanadate, 1× protease inhibitor mixture (without EDTA), pH 7. The SIP-ELISA (Echelon, ImTec Diagnostics, Antwerpen, Belgium) was performed according to the manufacturer's instructions. The absorbance at 450 nm was measured, and the concentration of SIP in the samples was determined by comparison with the standard curve as described (17).

Determination of cellular lipid peroxidation status

Lipid peroxidation was quantified by Bodipy 581/591 C11 (final concentration of 1 μM, 30 min, Thermo Fisher Scientific, Bremen, Germany) staining as described (46). The entire process was performed in the dark. Stained INSIE cells from the medium as well as from the dishes (after trypsinization) were collected by centrifugation at 700 × g for 3 min and resuspended in ice-cold PBS. After two washes, samples were measured using the CyFlow ML cytometer (Partec, Münster, Germany). For each sample, 20,000 events were acquired and analyzed by FlowJo software (Tree Star, Ashland, OR). Lipid peroxidation was defined as the ratio of the mean fluorescence in the FL-1 channel (488 nm/527 nm) and the FL-3 channel (488 nm/620 nm). Data are expressed as the fold change of lipid peroxidation of INSIE-ctr cells.

Lipidomics

Lipids were extracted as previously described (47). Samples were mixed for 2 min after addition of methanol (190 μl) and of 10 μl internal standard mix (0.1 μM SIP; 0.3 μM Sph, Cer 15:0 LPC 17:0, PC 17:0/17:0, SM 17:0, 5 μM LPE 17:1, PE 17:0/17:0, (Avanti Polar Lipids Inc, Alabaster, AL), as well as 10 μM d31-palmitic acid, d9-oleic acid and d5-hexadecanal and 3 μM Ergosterol (Cayman, Ann Arbor, MI) in methanol). Then, samples were centrifuged (21,300 × g, 4°C, 5 min), and the supernatant was transferred into mass spectrometry sample vials and stored at –80°C until measurement.

Prior to measurement, 100 μl aliquots of the supernatant were mixed with methanol (70 μl), 30 μl dansyl hydrazine (75 mM in MeOH), 30 μl EDC·HCl (525 mM in MeOH), and 30 μl pyridine (3 mM in MeOH) and vortexed for 2 h at room temperature. Following addition of formic acid (3 μl), samples were incubated for 30 min at room temperature and concentrated by vacuum centrifugation (1,450 rpm, 40°C, 1 h). Residues were dissolved in acetonitrile (100 μl), transferred

rabbit, a double immunostaining for parallel detection of SPL and SGPP1 in the same cells was not possible). Shown are Means ± SEM from four independent samples. ANOVA followed by Bonferroni, * $P < 0.05$, ** $P < 0.01$, *** $P < 0.001$ versus INSIE-control cells. The magnitude of SPL and SGPP1 overexpression was regularly checked during the entire time of cell culture.

into mass spectrometry vials, and stored at -80°C until measurement.

Chromatographic separation was performed on a LCMS-8050 triple quadrupole mass spectrometer (Shimadzu Duisburg, Germany) interfaced with a Dual Ion Source and a Nexera X3 Front-End-System (Shimadzu Duisburg, Germany). Chromatographic separation for SIP, sphingosine, and ceramides was performed with a 2×60 mm MultoHigh-C18 RP column with $3 \mu\text{m}$ particle size at 40°C . Mobile phases consisted of [A] methanol and [B] aq. Formic acid (1% v/v) and the following gradient settings were used: [A] increased from 10% to 100% over 3 min (B.curve = -2) and returned to 10% from 8.01 min to 10 min prior to next injection. MS settings for SIP and sphingosine were the following: Interface: ESI, nebulizing gas flow: 3 L/min, heating gas flow: 10 L/min, interface temperature: 300°C , desolvation temperature: 526°C , desolvation line temperature: 250°C , heat block temperature: 400°C , drying gas flow: 10 L/min. MS settings for ceramide and steroids were the following: Interface: APCI, nebulizing gas flow: 2.4 L/min, heating gas flow: 3 L/min, interface temperature: 300°C , desolvation temperature: 526°C , desolvation line temperature: 250°C , heat block temperature: 400°C , drying gas flow: 3 L/min. Flow rate was 0.4 ml/min. Data were collected using multiple reaction monitoring (MRM), and positive ionization was used for qualitative analysis and quantification. Standard curves were generated by measuring increased amounts of analytes (10 nM–5 μM SIP, Sph, Cer 14:0, 16:0, 18:0, 18:1, 20:0, 22:0, 24:0, 24:1) with internal standard (SIP-d7 = 0.1 μM ; Sph-d7, Cer 15:0 = 0.3 μM). Injection volume of all samples was 10 μl . The following MRM fragment ions (positive mode) were used for quantification: $m/z = 264$ and 82 for SIP, $m/z = 252$ for sphingosine, and $m/z = 264$ for Cer.

Mobile phases for phosphoglyceride, sphingomyelin, and fatty acid/aldehyde measurement consisted of [A] 10 mM aq. ammonium formate + 0.01% (v/v) formic acid and [B] acetonitrile + 0.01% (v/v) formic acid/isopropanol (1:1). Phosphoglyceride and sphingomyelin profiling was performed with a 3×150 mm Accucore Polar Premium column with $2.6 \mu\text{m}$ particle size and the following gradient settings were used: 20% [B] from 0 min to 1 min, 20%–40% [B] from 1 min to 2 min, 92.5% [B] from 2 min to 25 min, 100% [B] from 26 min to 35 min, and return to 20% [B] from 35.1 min to 38 min prior next injection. Data were collected using MRM. Positive ionization was used for quantification and standard curves were generated by measuring increased amounts of analytes (0.1 μM –10 μM , LPC 14:0, 16:0, and 18:0; PC 32:0, 34:1, 34:2, 36:0, 36:4, 36:6, 38:4, and 40:6; LPE 16:0, 18:0; PE 16:0/18:1; SM 32:1, 34:1, 36:1, 42:1 and 42:2) with internal standards (3 pmol LPC 17:0, PC 17:0/17:0, SM 17:0, 30 pmol LPE 17:1, PE 17:0/17:0). Fatty acid/aldehyde profiling was performed with a 2×60 mm MultoHigh-C8 RP column with $3 \mu\text{m}$ particle size at 40°C and the following gradient settings were used: 40%–5% [B] from 0 min to 9.5 min (B.Curve = -2), 5% [B] to 0% [B] from 9.5 min to 12.0 min, and equilibration from 12.01 min to 15 min prior next injection. Flow rate was 0.4 ml/min and injection volume was 3 μl . MRM fragment ion $m/z = 171$ in ESI(+) mode was used for quantification and standard curves were generated by measuring increased amounts of analytes (0.1 μM –30 μM 2-HDE, HDA; 1 μM –300 μM fatty acid 16:0, 18:1) Linearity of standard curves and correlation coefficients were obtained by linear regression analysis. All MS analyses were performed with software LabSolutions 5.114 and LabSolutions Insight (Shimadzu, Kyoto, Japan) and further processed in Microsoft Excel. Data are shown as Means \pm SEM in pmoles/sample.

Data analysis

All data are expressed as Means \pm SEM. Statistical analyses were performed using the Prism analysis software (Graphpad, San Diego, CA) using *t* test or ANOVA followed by Bonferroni correction, with $P < 0.05$ considered statistically significant.

RESULTS

Overexpression of SIP enzymes catalyzing SIP turnover in insulin-secreting INSIE cells

To further validate the role of intracellular SIP in lipotoxicity in pancreatic beta-cells, we used insulin-secreting INSIE cells. These cells abundantly express Sk2 and Sgpp2, while Sgpp1 and Spl are hardly detectable (8, 17, 24), making them a useful model for studying the consequences of an augmented SPL and SGPP1 expression. INSIE cells were genetically modified to overexpress human SPL (8, 17) or human SGPP1. The expression of SPL and of SGPP1 was significantly elevated as revealed by measurements at the level of mRNA (human SPL and SGPP1) and protein (Western blot and immunofluorescence) (Fig. 1A and C). The expression of Sk2 and Sgpp2 was differentially affected by SPL versus SGPP1 overexpression (Fig. 1A), suggesting that changes in intracellular SIP turnover capacity may affect the expression of sphingolipid pathway enzymes. Furthermore, we observed a strongly reduced SIP concentration in the cell lysates of INSIE-SPL cells (approx. 60% reduction) but somewhat smaller 40% decrease of SIP content in INSIE-SGPP1 cells than INSIE-ctr cells (Fig. 1B). Consistent with previous reports, our result indicates that both overexpressed enzymes were active with SPL being slightly more efficient in reducing the cellular SIP than SGPP1 (48), probably due to a stronger Sk2 and a weaker Sgpp2 expression in INSIE-SGPP1 cells enabling a partial regeneration of the cellular SIP pool. Since the concentration of hexadecenal was below the detection limit (see below), we estimated the capacity of SPL to generate the reaction products indirectly by the assessment of phosphatidylethanolamine (PE) levels. PE is generated by different pathways within cells. It has been shown, however, that the amount of PE is significantly affected by changes in the enzymatic activity of SPL (49) as only one enzymatic step is needed to generate PE from ethanolamine phosphate, the second reaction product of SPL. Indeed, PE levels were elevated in INSIE-SPL cells, whereas they were reduced in INSIE-SGPP1 cells as compared to INSIE-ctr cells (Fig. 1B) strongly indicating higher SPL and SGPP1 activities, respectively.

Enhanced SIP turnover modulates the effects of FFA on sphingolipid metabolism in insulin-secreting INSIE cells

Because we observed compensatory changes in SIP metabolic enzyme expression in cells overexpressing SPL and SGPP1, we analyzed the impact of SIP turnover

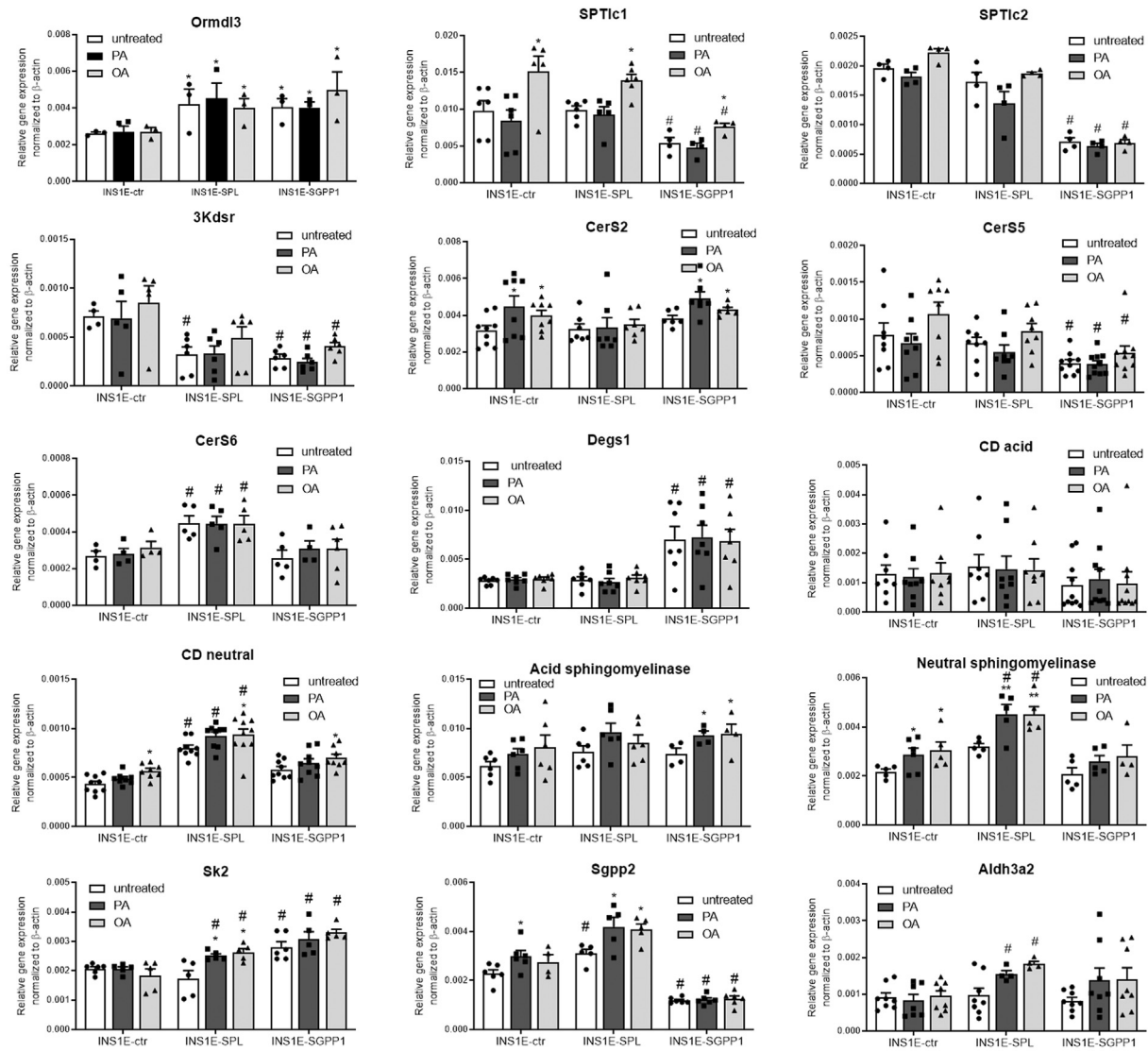
on sphingolipid pathway enzyme expression and sphingolipid metabolism under control conditions and in the presence of FFA. We exposed cells to the most physiologically relevant and abundant FFA, namely saturated PA (500 μ M) or monounsaturated OA (500 μ M) for 24 h. These concentrations of FFA are standard effective concentrations used in rodent beta-cells with well-described effects upon a 24 h exposure (8, 9, 39, 46).

The major regulation of sphingolipid de novo biosynthesis occurs post translationally via ORMDL proteins, of which ORMDL3 is abundantly expressed in beta-cells (Fig. 2). Overexpression of SPL or SGPP1 significantly increased the mRNA expression of Ormdl3, without any significant effect of FFA treatment (Fig. 2A). Former studies indicate that ORMDL3 gene and protein expression levels are not always concordant, which suggests that ORMDL3 might be differentially regulated on the transcriptional versus translational levels (50). Indeed, translation of Ormdl3 mRNA was not always congruent with the amount of transcript (Fig. 2A and B). As depicted in Figure 2B, Ormdl3 protein expression was somewhat lower in INSIE-SGPP1 than other untreated cells. FFA treatment did not significantly influence the translation of Ormdl3 transcript in any analyzed cell clones (Fig. 2B). This result prompted us to analyze possible adjustments of sphingolipid biosynthesis and degradation capacity that could contribute to FFA toxicity in these cells. We started with the serine palmitoyl transferase (SPT), the rate-limiting enzyme of de novo sphingolipid biosynthesis, which converts L-serine and palmitoyl-CoA to 3-oxosphinganine. We determined the mRNA level of both SPT long chain (SPTlc) subunits 1 and 2 required for enzymatic activity. The expression of SPTlc1 was not affected by PA but significantly upregulated by OA in all analyzed cell clones (Fig. 2). The expression of SPTlc1 was, however, significantly lower in INSIE-SGPP1 cells than in INSIE-ctr and INSIE-SPL cells (Fig. 2). SPTlc2 expression was not affected by FFA exposure but was strongly reduced by SGPP1 overexpression (Fig. 2). This result indicates a reduced rate of de novo sphingolipid biosynthesis in INSIE-SGPP1 cells. The mRNA expression of 3-ketodehydrospingosine reductase catalyzing the reduction of 3-oxosphinganine to sphinganine was significantly lower in untreated INSIE-SPL and INSIE-SGPP1 cells than in control cells (Fig. 2), with a weak tendency of elevated expression following OA exposure (Fig. 2). N-acylation of sphinganine to dihydroceramide is catalyzed by three of the six known ceramide synthase isoforms, namely CerS2, CerS5, and CerS6, predominantly expressed in INSIE cells. The effects of SPL and SGPP1 overexpression as well as of FFA treatment on the mRNA expression of these enzymes are rather heterogenous. Thus, CerS2 expression was not affected neither by SPL nor by SGPP1 overexpression but was elevated by FFA treatment in

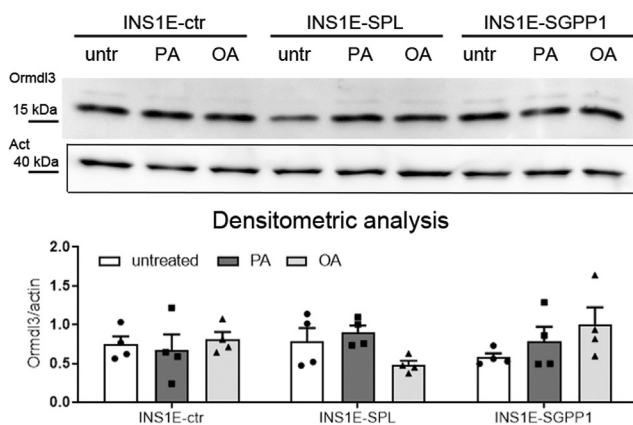
INSIE-ctr and INSIE-SGPP1 cells. However, CerS5 expression was considerably reduced in INSIE-SGPP1 cells as compared to control and SPL overexpressing cell clones, while the expression of CerS6, which is responsible for ceramide formation in mitochondria, was significantly upregulated only in INSIE-SPL cells independently of FFA treatment (Fig. 2). On the other hand, the expression of sphingolipid-delta-4-desaturase (Degs1), catalyzing the formation of ceramide from dihydroceramide, was significantly higher in INSIE-SGPP1, but not affected by FFA (Fig. 2). Next, we analyzed the transcript amounts of two enzymes catalyzing ceramide hydrolysis in different cellular compartments at different pH optima. Acid ceramidase (CD), which is mainly localized to the lysosomes, was affected neither by overexpression of SPL and SGPP1 nor by FFAs treatment. Yet, the expression of neutral CD, which is active in various cellular membranes, was significantly increased by SPL overexpression as well as by OA treatment (Fig. 2). We then determined the amount of acid and neutral sphingomyelinase mRNA, as these two enzymes are known to generate ceramide from sphingomyelin, one of the most abundant sphingolipids in cellular plasma membranes (15). While expression levels of the lysosomal enzymes acid sphingomyelinase and acid CD were not affected by the different conditions, the expression of neutral sphingomyelinase was significantly increased by FFA treatment especially in SPL-overexpressing cells (Fig. 2). Similar to neutral CD, neutral sphingomyelinase was not affected in SGPP1-overexpressing cells independently of FFA treatment (Fig. 2). We then analyzed the expression of two enzymes directly involved in SIP metabolism. The expression of SK2, which phosphorylates sphingosine yielding SIP, was strongly elevated on the one hand by SGPP1 overexpression and on the other hand by PA and OA treatment but only of INSIE-SPL cells (Fig. 2). The expression of SGPP2, the predominant SIP phosphatase isoform in beta-cells, was significantly elevated in SPL overexpressing cells but considerably reduced in SGPP1 overexpressing cells (Fig. 2). PA treatment also increased SGPP2 expression in control and SPL overexpressing cells, whereas OA treatment had a similar increasing effect but only in INSIE-SPL cells (Fig. 2). Finally, we analyzed the expression of the aldehyde dehydrogenase 3 family member A2 (Aldh3a2), the enzyme that rapidly oxidizes hexadecenal, a rather toxic product of the SPL reaction, to form palmitoleic acid. Aldh3a2 was strongly expressed in all analyzed INSIE cell clones (Fig. 2A and B). Interestingly, FFA tended to elevate the Aldh3a2 protein expression in INSIE-SPL cells (Fig. 2B), indicating that under lipotoxic stress, INSIE-SPL cells might be equipped with a better hexadecenal detoxification capacity.

We then performed a lipidomic analysis to check whether and how the observed changes in the expression of sphingolipid pathway enzymes affected the

A Gene expression of regulators and enzymes of the sphingolipid pathway



B Ormdl3 protein expression



Aldh3a2 protein expression

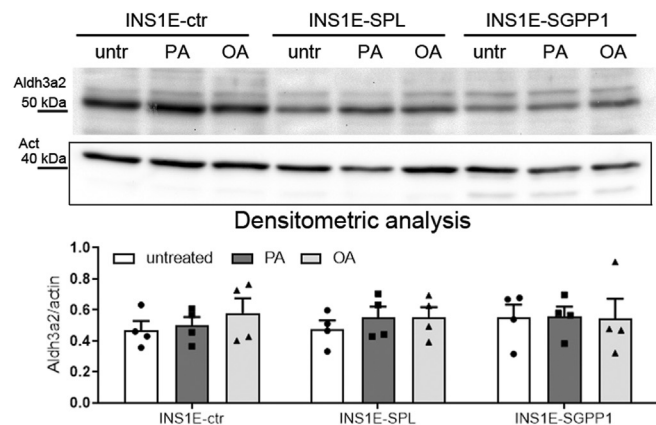


Fig. 2. Effects of an increased SIP turnover on FFA-mediated changes of the expression of enzymes of the sphingolipid pathway in insulin-secreting INSIE cells. INSIE-ctr, -SPL and SGPP1 cells were incubated in the absence or presence of PA or OA (each of 500 μ M) for 24 h. Thereafter (A) RNA was isolated, cDNA was synthesized and real-time PCR was performed. Shown are MEANS \pm SEM from $n = 4-8$ independent experiments, each condition was measured in triplicates. (B) protein expression was analyzed by Western blotting, shown are representative blots and densitometry analysis of protein expression normalized to β -actin of $n = 4$ individual experiments. ANOVA followed by Bonferroni, * $P < 0.05$, ** $P < 0.01$, *** $P < 0.001$ versus untreated, # $P < 0.05$ versus INSIE-ctr cells treated in the same way.

amount of certain lipid species (Fig. 3). First, we measured PA and OA content and observed significantly lower levels in untreated INSIE-SPL and INSIE-SGPP1 as compared to control cells. As expected, incubation of cells with PA and OA, respectively, caused an increase of the respective FA (Fig. 3). The measurements of sphingosine revealed a significantly lower level in untreated INSIE-SPL cells as compared to control and SGPP1 cells (Fig. 3). While OA increased sphingosine content in all analyzed clones, PA affected sphingosine levels differentially. PA did not affect the sphingosine content in INSIE-ctr, while it tended to upregulate it in INSIE-SGPP1 cells (Fig. 3). Only in the INSIE-SPL cells, PA strongly enhanced sphingosine content (Fig. 3). SIP content was significantly increased by OA treatment in INSIE-ctr cells (Fig. 3). No significant effects of FFA incubations on SIP levels in INSIE-SPL or SGPP1 cells were detected (Fig. 3). Importantly, we were unable to detect hexadecenal in INSIE-ctr and SGPP1 cells, consistent with the low expression of SPL in these cells. Also, in untreated or FFA-treated INSIE-SPL cells, no hexadecenal could be detected, strongly indicating that the abundant expression of Aldh3a2 (Fig. 2) was able to efficiently remove the toxic aldehyde. Interestingly, we observed profound differences in the ceramide species profile in response to FFA between the clones examined. The content of various sphingomyelins was decreased in response to PA in INSIE-ctr and SPL cells and to a lesser extent in INSIE-SGPP1 cells (Fig. 3).

Together, our results show that both manipulated SIP metabolism and FFA treatment affect sphingolipid metabolism in an additive or independent manner. The observed changes suggest moreover, that the transcription of enzymes involved in sphingolipid metabolism is controlled by *i*) dietary FFA, *ii*) intracellular SIP levels, and/or *iii*) other bioactive sphingolipids closely associated with SIP and FFA metabolism.

Upregulation of SIP recycling has opposite effects on beta-cell susceptibility to FFA to those caused by enhanced SIP degradation in insulin-secreting INSIE cells

The analysis of cell viability confirmed a well-known toxic effect of PA (500 μ M) and the lack of toxicity of OA (500 μ M) in INSIE-ctr cells (Fig. 4A). In line with our earlier findings, SPL overexpression significantly potentiated PA-induced loss of cell viability. That was in contrast to the nearly complete lack of toxic effect of PA in INSIE-SGPP1 cells (Fig. 4A). Interestingly, the incubation with OA led to a significant decrease of cell viability both in INSIE-SPL and – to a lesser extent – in INSIE-SGPP1 cells (Fig. 4A). Similar, but slightly weaker effects of SPL versus SGPP1-overexpression were visible upon exposure to lower FFA concentrations (250 μ M) and the mixture of PA+OA (500 μ M) (supplemental Fig. S1). In the subsequent experiments, we decided to focus on the opposite effects of PA

versus OA at the higher concentrations, the approach which allows a direct and clear comparison of a differential role of SIP turnover capacity on lipotoxicity in beta-cells indicative for effects related to diets enriched in saturated versus unsaturated FFA.

The MTT assay strongly depends on total mitochondrial activity, which mirrors the number of cells for most cell populations. To investigate whether the effects observed in the MTT assay correlated with induction of apoptosis, we employed caspase-3-cleaved assay. PA induced caspase-3 activation in INSIE-ctr and even more strongly in INSIE-SPL cells but failed to induce apoptosis in INSIE-SGPP1 cells (Fig. 4B). OA did not induce caspase-3 activation in INSIE-ctr and INSIE-SGPP1 cells but slightly increased caspase-3 cleavage in INSIE-SPL cells (Fig. 4B).

Finally, we studied the differential effects of SPL versus SGPP1 overexpression on the expression of Chop (C/EBP homologous protein), an ER stress marker that is induced by lipotoxicity in beta-cells and is believed to play an important role in beta-cell death (51). The fact that overexpression of SPL and SGPP1 did not increase Chop expression in untreated cells argues against their role as trigger of the ER stress response. Confirming earlier studies, we found that PA was a particularly strong inducer of Chop expression in control INSIE cells (Fig. 4C). The PA-mediated effects were potentiated by SPL overexpression in line with our earlier observations (8), but not by SGPP1 overexpression (Fig. 4C). The Chop expression was weakly induced by PA in INSIE-SGPP1 cells (Fig. 4C).

Differential effects of enhanced SIP turnover on oxidative stress and identification of intracellular sources of ROS in insulin-secreting INSIE cells

Next, we investigated the oxidative stress response, which is believed to play a crucial role in the toxicity of lipids in beta-cells (2, 5, 9, 10, 46, 52–54). We analyzed the overall oxidative stress using a robust DCFDA-based assay, which enables the detection of increased generation of a variety of reactive oxygen species (ROS). A significant induction of oxidative stress in INSIE-ctr cells exposed to PA, but not to OA, was detected (Fig. 5A). Interestingly, SPL overexpression was associated with a significantly stronger induction of ROS generation in both PA- and OA-treated cells, as compared to INSIE-ctr cells (Fig. 5A). Neither PA nor OA induced oxidative stress in INSIE-SGPP1 cells (Fig. 5A). In line with these observations, we observed an induction of H₂O₂ generation in response to PA in all analyzed cell clones using the hydrogen peroxide-specific fluorescence sensor protein HyPer expressed in the cytosolic cell compartment, which was, however, hardly detectable in INSIE-SGPP1 cells (Fig. 5B). The fluorescence emitted from HyPer sensor protein changes from green (low H₂O₂) to red (high H₂O₂ concentration) upon generation of H₂O₂. In INSIE-ctr cells, we observed some areas of yellow/orange

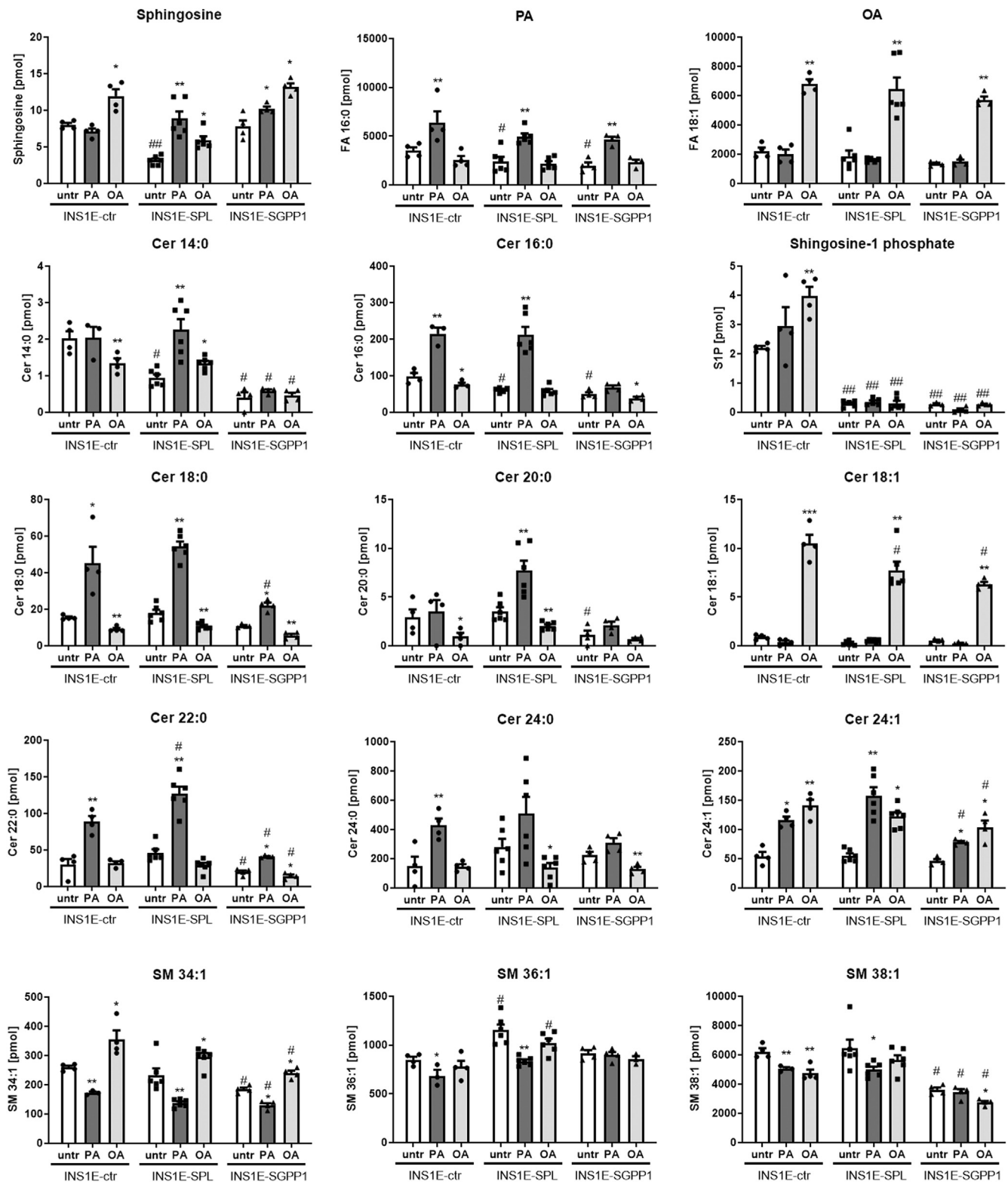


Fig. 3. Effects of an increased SIP turnover in insulin-secreting INSIE cells on lipid species after exposure to FFA. INSIE cells were incubated in the absence or presence of PA or OA (500 μ M of each) for 24 h. Thereafter, lipids (sphingosine, SIP, PA, OA, Cer = ceramide, SM = sphingomyelin) were extracted and analyzed by mass-spec as described in Methods. Shown are Means \pm SEM from $n = 3-6$ independent experiments. ANOVA followed by Bonferroni, * $P < 0.05$, ** $P < 0.01$, *** $P < 0.001$ versus untreated, # $P < 0.05$ versus INSIE-ctr cells treated in the same way.

fluorescence in cytoplasm with a dot-like pattern of red fluorescence upon exposure to PA (Fig. 5B). In INSIE-SPL cells treated with PA, big areas of cytoplasm were

red indicating that H_2O_2 concentration increase was higher than in INSIE-ctr cells and that its distribution was much more widespread throughout the entire cells

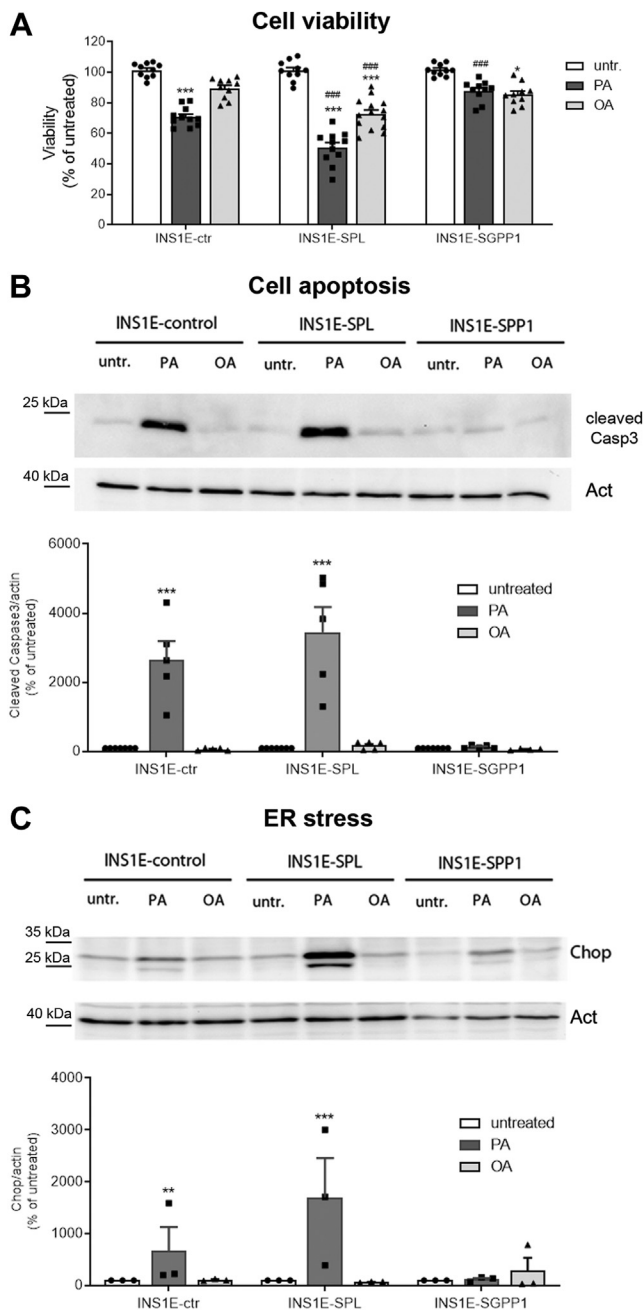


Fig. 4. Effects of an increased SIP turnover in insulin-secreting INSIE cells on cell viability, apoptosis, and ER stress after exposure to FFA. INSIE cells were incubated in the absence or presence of PA or OA (500 μ M of each) for 24 h. Thereafter, (A) cell viability was measured by MTT assay, (B) activation of caspase-3 was detected by Western blot analysis of cleaved caspase-3 protein expression, and (C) induction of Chop was detected by Western blot analysis. Shown are representative WBs and a densitometry analysis of protein expression detected in all experiments. Shown are Means \pm SEM from $n = 3-6$ independent experiments, each condition was measured in triplicates. ANOVA followed by Bonferroni. * $P < 0.05$, ** $P > 0.01$, *** $P < 0.001$ versus untreated, #### $P < 0.001$ versus INSIE-ctr cells treated in the same way.

(Fig. 5B). In response to OA, a minor increase in H_2O_2 formation was observed only in INSIE-SPL cells expressing the HyPer-Cyto protein (Fig. 5B).

To identify the subcellular sources of H_2O_2 generation, we expressed the HyPer sensors in peroxisomes and in mitochondria. Peroxisomes are considered the main source of H_2O_2 generation upon PA exposure in beta-cells. As anticipated, a strong induction of peroxisomal H_2O_2 generation was detected in response to PA in INSIE-ctr cells, which was further potentiated by SPL overexpression (Fig. 6A). In INSIE-SPL cells incubated with OA, a slightly increased red fluorescence of the HyPer-Peroxi protein was visible (Fig. 6A). In INSIE-SGPP1 cells, no induction of peroxisomal H_2O_2 generation was observed (Fig. 6A).

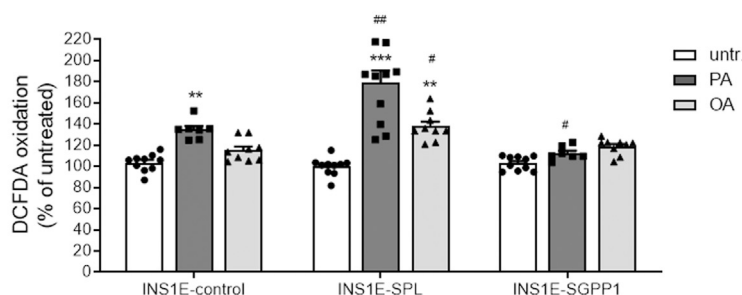
FFA are believed to mildly elevate mitochondrial H_2O_2 formation as a result of their mitochondrial metabolism, but not related to any toxic effect, with the exception of very long chain FFAs (5). This observation was confirmed in our study in INSIE-ctr cells (Fig. 6B). Interestingly, we observed increased red fluorescence in the HyPer-Mito protein expressed in INSIE-SPL cells exposed to PA and to a lesser extent also in INSIE-SPL cells incubated with OA (Fig. 6B), indicating high concentrations of H_2O_2 under these conditions. Moreover, the pattern of the HyPer-Mito staining was suggestive of mitochondrial damage in FFA-treated INSIE-SPL cells. Again, no increase in mitochondrial H_2O_2 formation was detected in INSIE-SGPP1 cells (Fig. 6B).

Turnover of intracellular SIP affects mitochondrial stress and ceramide generation in response to FFA in insulin-secreting INSIE cells

Since we observed signs of mitochondrial network fragmentation in FFA-exposed INSIE-SPL cells and an elevated H_2O_2 formation was detected, we further explored the mitochondrial network and mitochondrial stress markers. Using the MitoTracker Deep RedTM staining technique, we analyzed changes in the mitochondria network structure in response to FFA (Fig. 7A). PA induced the formation of round-shaped mitochondria in INSIE-ctr cells, however in a much stronger manner in INSIE-SPL cells, in which large aggregates of mitochondria could additionally be detected (Fig. 7A). Exposure to OA of INSIE-SPL cells caused milder effects but also resulted in the defective mitochondrial network appearance (Fig. 7A). In contrast, the mitochondrial network was enlarged and elongated in untreated and FFA-treated INSIE-SGPP1 cells.

Next, we analyzed the expression of mitochondrial proteins that could be involved in the regulation of oxidative stress, mitochondrial function, as well as in mitochondrial unfolded protein response (UPR^{mt}). Interestingly, the expression of MnSOD, the mitochondrial isoform of superoxide dismutase, was significantly higher in INSIE-SPL cells than in other analyzed cell clones, and additionally enhanced by PA (Fig. 7B). The expression of Lonpl1, a mitochondrial ATP-dependent serine protease that mediates the selective degradation of misfolded, unassembled, or

A Overall oxidative stress



B Cytosolic generation of hydrogen peroxide

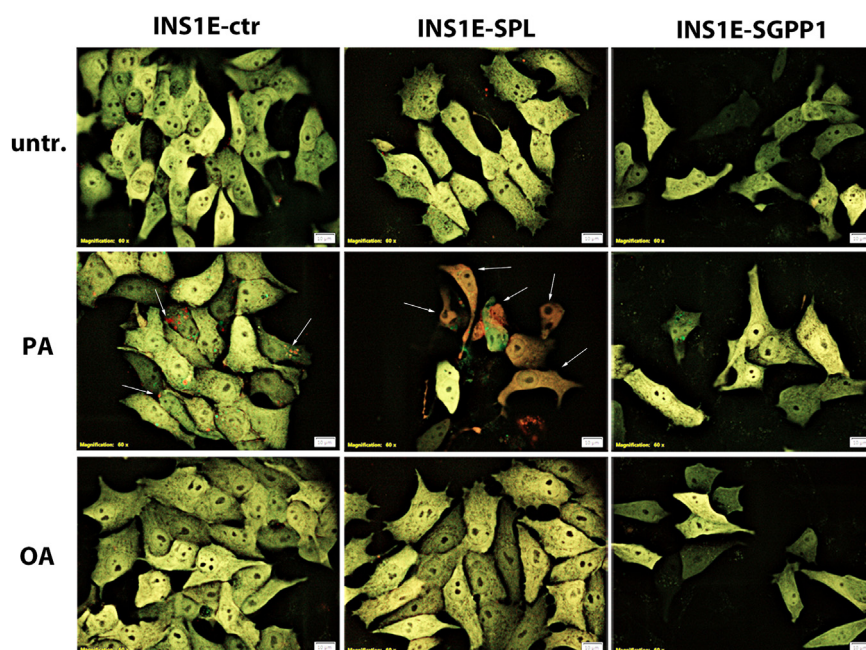


Fig. 5. Effects of enhanced SIP turnover and FFA on overall oxidative stress and cytosolic hydrogen peroxide production in insulin-secreting INSIE cells. INSIE cells were incubated in the absence or presence of PA or OA (500 μM of each) for 24 h. (A) overall oxidative stress was measured by DCFDA method. (B) cytosolic hydrogen peroxide generation was estimated by expressing the hydrogen peroxide-sensitive fluorescence sensor HyPer-Cyto protein in the cytosolic compartment of cells and evaluation of fluorescence shift by the CellSens software at the Olympus fluorescence microscope (representative pictures from $n = 3$ individual experiments), Bars: 10 μm. Shown (A) are Means \pm SEM from $n = 3$ –6 independent experiments, each condition was measured in triplicates ANOVA followed by Bonferroni, ** $P < 0.01$, *** $P < 0.001$ versus untreated, # $P < 0.05$, ## $P < 0.01$, versus INSIE-ctr cells treated in the same way.

oxidatively damaged polypeptides, and which is induced by oxidative stress, was increased in INSIE-ctr cells by FFA treatment (Fig. 7B). INSIE-SPL cells were characterized by an abundant basal expression of Lonpl, which was upregulated by FFA (Fig. 7B). A significantly lower expression of Lonpl was detected in INSIE-SGPP1 cells. Prohibitin 2 (Phb2), an inner mitochondrial membrane protein that is involved in protection against oxidative damage, regulation of mitophagy, and ATP biosynthesis, was increased by PA and to a lesser extent by OA in INSIE-ctr cells (Fig. 7B). Confirming our earlier observations (17), we detected a higher basal expression of Phb2 in INSIE-SPL cells as

compared to INSIE-ctr cells with no additional effect upon FFA treatment (Fig. 7B). In INSIE-SGPP1 cells, the expression of Phb2 protein was significantly lower than in INSIE-SPL cells, and it was not influenced by exposure to FFA (Fig. 7B).

The observed changes in mitochondrial network formation and mitochondrial proteins indicate an activation of mitochondrial stress response after treatment with FFA particularly in INSIE-SPL cells, whereas overexpression of SGPP1 obviously protected the cells against these deleterious effects. Mitochondrial stress results in a loss of adequate ATP generation. Indeed, in cells exposed to FFA for 24 h, PA decreased ATP

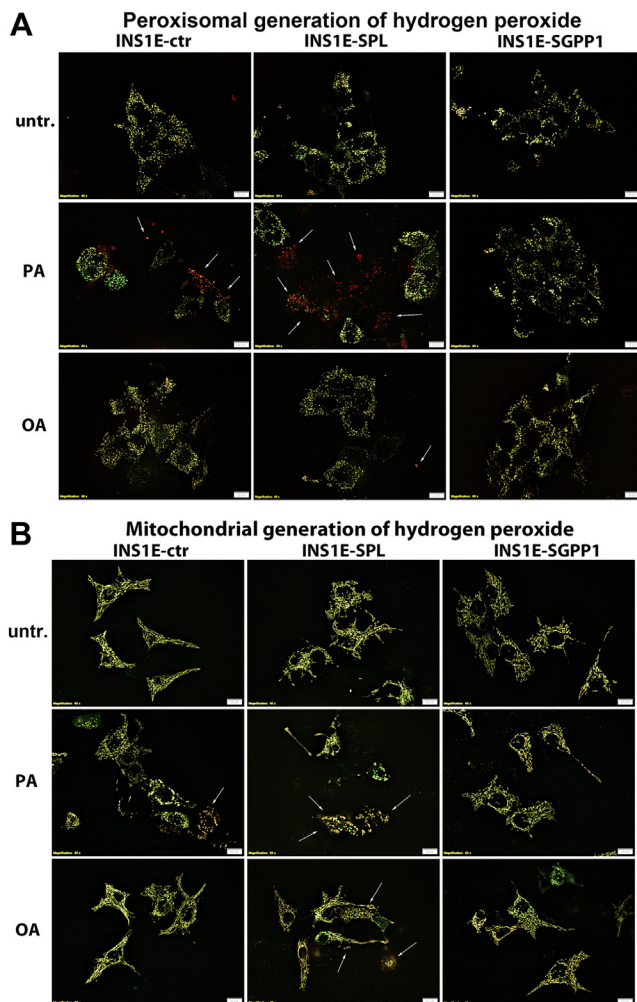


Fig. 6. Effects of enhanced SIP turnover and FFA on peroxisomal and mitochondrial hydrogen peroxide production in insulin-secreting INSIE cells. INSIE cells were incubated in the absence or presence of PA or OA (500 μ M of each) for 24 h. Peroxisomal hydrogen peroxide generation was estimated by expressing the fluorescence sensor HyPer-Peroxi (A) and mitochondrial by expressing HyPer-Mito (B) sensor proteins and evaluation of fluorescence shift by the CellSens software at the Olympus fluorescence microscope (representative pictures from $n = 3$ individual experiments). Arrows depict representative cells with higher red HyPer protein fluorescence. Bars: 10 μ m.

content (by around 25%) in INSIE-ctr cells and even more in INSIE-SPL cells (by around 40%) (Fig. 7C). While OA did not affect ATP content significantly in INSIE-ctr cells, it led to a significant drop in ATP content in INSIE-SPL cells by about 15% (Fig. 7C). INSIE-SGPP1 cells were characterized by a lower basal ATP content than INSIE-ctr or INSIE-SPL cells, which was, however, not influenced by FFA (Fig. 7C).

Mitochondrial function and survival have been shown to be regulated by formation and accumulation of proapoptotic ceramide species (55). In INSIE-SPL cells treated with FFA, we observed higher neutral sphingomyelinase and CerS6 expression levels that could favor the observed ceramide increase,

particularly in the mitochondria. Ceramide is synthesized at the ER and translocated by CERT1 to the Golgi compartment for conversion to sphingomyelin (56, 57). A disturbed or lower capacity of ceramide transport to the Golgi could favor ceramide transport to mitochondria and its intramitochondrial accumulation. Yet, the expression of Cert1 in INSIE-ctr cells was not affected by FFA (Fig. 7D). Interestingly, in INSIE-SPL cells, a significantly lower expression of Cert1 was observed, which was not further influenced by FFA (Fig. 7D). The expression of Cert1 in INSIE-SGPP1 cells was high and, similarly to other cell clones, not affected by FFA (Fig. 7D). Finally, using a well-established immunofluorescence ceramide staining (green) together with the MitoTracker staining (red), we visualized ceramide content of cells exposed to FFA with a particular focus on its mitochondrial localization (Fig. 7E). Ceramide content was increased in response to PA in INSIE-ctr and INSIE-SPL cells, but not in INSIE-SGPP1 cells (Fig. 7E). Interestingly, in INSIE-SPL cells, we observed that ceramide tended to accumulate in the vicinity of mitochondria, while in INSIE-ctr cells, such a colocalization was rather rarely observed (Fig. 7E). A colocalization of ceramide and mitochondria was observed in OA-treated INSIE-SPL cells, however to a lower extent than in PA-treated cells (Fig. 7E).

Together, these results indicate that lipid distribution and use in beta-cells exhibiting an increased irreversible SIP degradation capacity is remarkably distinct from those with enhanced SIP recycling, significantly impacting mitochondrial dysfunction in response to FFA.

Distinct effects of SIP recycling versus degradation on LDs formation, but similar on lipid peroxidation in insulin-secreting INSIE cells

Since we observed a distinct lipid distribution pattern in cells overexpressing SPL versus SGPP1, in the next step, we analyzed the lipid storage capacity of cells treated with FFA. During LD biogenesis, neutral lipids (e.g., triglycerides) accumulate within the ER bilayer, with rising concentrations leading to the formation of LD. An insufficient capacity of LD formation may lead to lipid overload of the ER, a process that can contribute to ER stress induction. The LD biogenesis is a complex process, for which the expression of several specific proteins, regulating bud formation, and lipid transfer, is crucial (58, 59). First, we assessed the expression of seipin, Dgat2, and Plin proteins that are essential for LD formation and function (58–60).

The expression of seipin was unaffected in INSIE-SPL cells while significantly elevated only in OA-treated INSIE-ctr and SGPP1 overexpressing cells (Fig. 8A). The basal expression of Dgat2, which catalyzes the synthesis of triacylglycerol (the main cellular neutral lipid) and interacts with LD at the ER side, was significantly higher in both SPL and SGPP1 overexpressing cells (Fig. 8B). However, treatment with FFA significantly

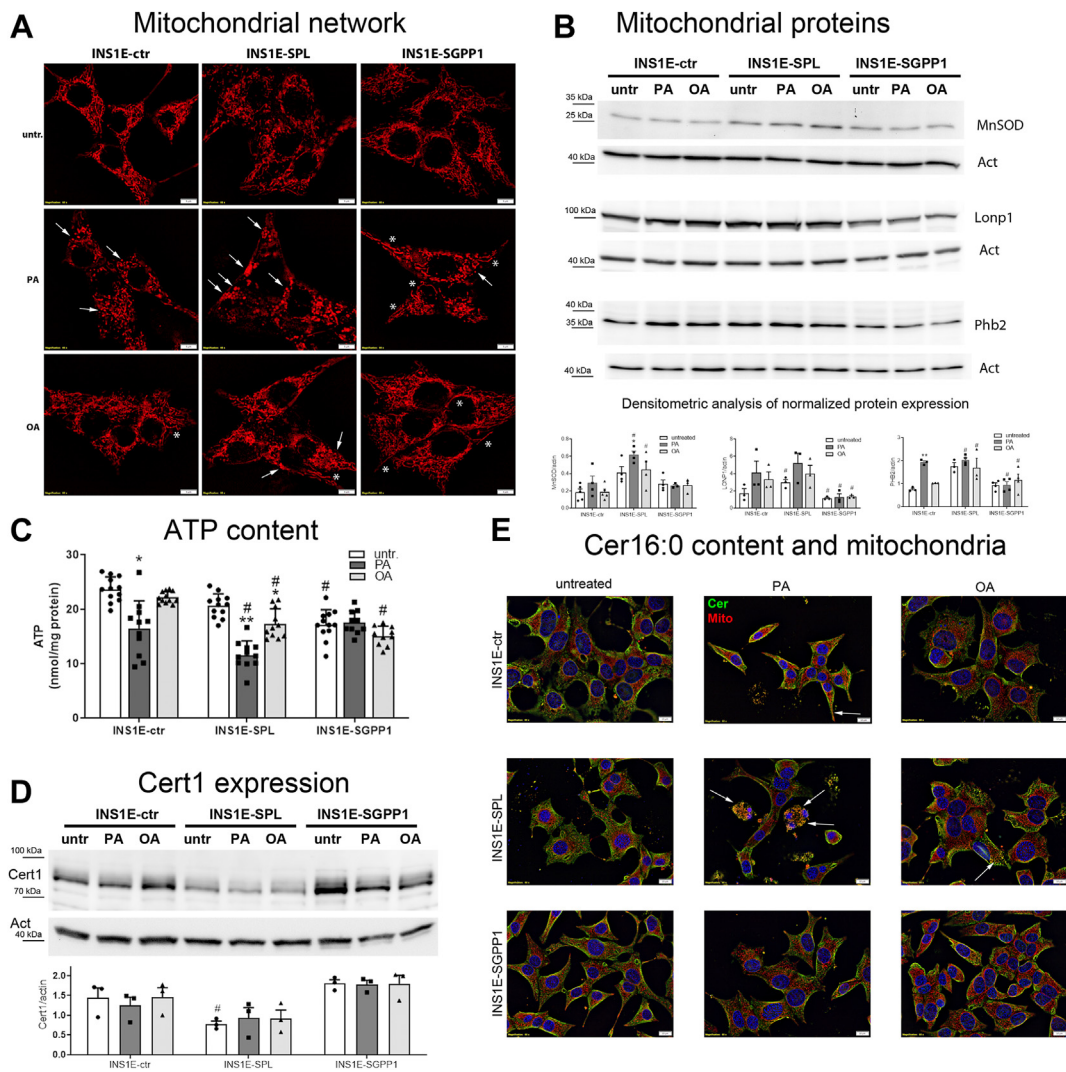


Fig. 7. Effects of SIP turnover and free fatty acids on mitochondrial network, stress, and metabolic activity in insulin-secreting INSIE cells. INSIE cells were incubated in the absence or presence of PA or OA (500 μ M of each) for 24 h. Thereafter, (A) mitochondrial network was analyzed after incubation with Mitotracker Deep Red™, Bars: 5 μ m, (B) the expression of proteins important for mitochondrial stress was measured by Western blot, (C) ATP content was measured by ATPlite assay, shown are Means \pm SEM from $n = 4$ independent experiments, each conditions was measured in triplicates. (D) Cert1 protein expression was analyzed by Western blot and (E) cellular distribution and content of ceramide (green) was performed by immunofluorescence in parallel with the MitoTracker Deep Red™ staining (red), Bars: 10 μ m. Arrows depict the areas of ceramide and mitochondria colocalization (yellow). Shown are representative pictures of $n = 3$ –5 independent experiments. Densitometry analyses of protein expression normalized to β -actin are shown as Means \pm SEM from $n = 3$ –5 independent experiments. ANOVA followed by Bonferroni, * $P < 0.05$, ** $P < 0.01$, *** $P < 0.001$ versus untreated, # $P < 0.05$, versus INSIE-ctr cells treated in the same way.

reduced its expression in INSIE-SGPP1 cells but had no additional effect in INSIE-SPL cells (Fig. 8B).

Apart of Plin2 and Plin3, known to be abundantly expressed in INSIE cells, we also detected Plin5 (Fig. 8C), in line with earlier reports (61). Consistent with our previous data, we found a significantly lower expression of Plin2 in INSIE-SPL cells (Fig. 8C). In contrast, INSIE-SGPP1 cells were characterized by an abundant Plin2 expression (Fig. 8C). As shown in Figure 8C, no striking modifications of Plin3 expression were detectable (Fig. 8C). Plin5 expression, on the other hand, was downregulated in SPL overexpressing cells and also in control cells treated with PA (Fig. 8C).

Next, we analyzed LD generation by Oil Red O staining and observed a strong induction of LD formation in response to OA in INSIE-ctr cells, as shown by an increased ratio of LD area/total cell area and by the presence of multiple LD puncta in cells (Fig. 8D and E). A significantly lower number of LDs in INSIE-SPL cells, but a significantly higher number of LDs in INSIE-SGPP1 cells, was detected after exposure to OA (Fig. 8D). These effects were dose-dependent (supplemental Fig. S1). Interestingly, in untreated and PA-treated INSIE-SGPP1 cells, we observed the presence of a high number of LDs (Fig. 8D). We then analyzed the ratio of very small, small, medium, and

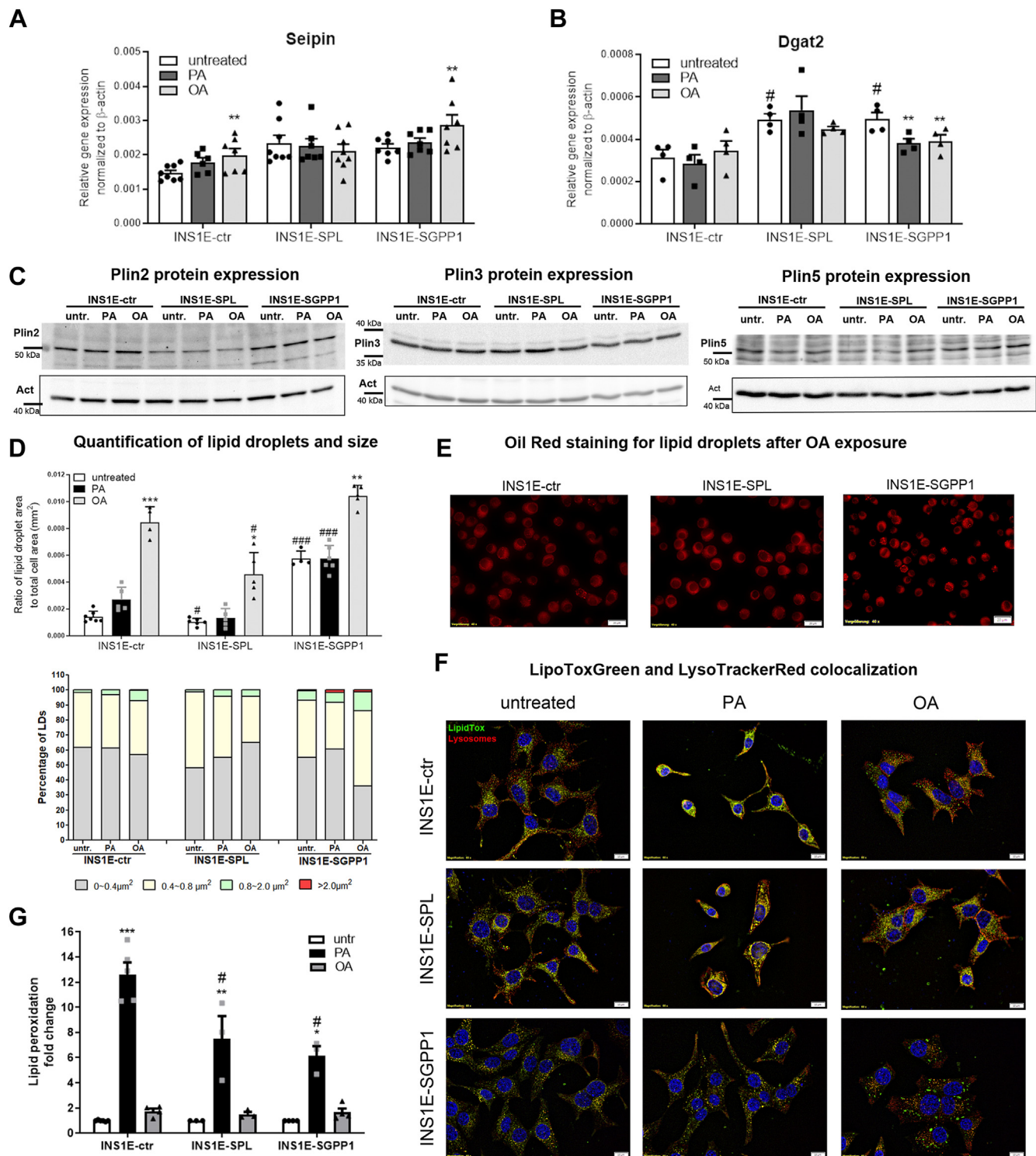


Fig. 8. Effects of SIP turnover and free fatty acids on lipid droplet formation, content, size, and autophagy as well as on lipid peroxidation in insulin-secreting INSIE cells. INSIE cells were incubated in the absence or presence of PA or OA (500 μM of each) for 24 h. Shown are (A) the gene expression of seipin by qRT-PCR, (B) gene expression of Dgat2 by qRT-PCR (Means \pm SEM from $n = 4-8$ independent experiments), (C) representative Plin2, Plin3, and Plin5 WBs from four independent experiments, (D) quantification of the number and size of lipid droplets after exposure FFA from $n = 4-7$ independent experiments, (E) lipid droplets detection by OilRed staining, a representative picture from $n = 4-7$ independent experiments, Bars: 20 μm , (F) colocalization of lipids (LipidTox Green) with lysosomes (LysoTracker Red), Bars: 10 μm , (G) lipid peroxidation, Means \pm SEM from four independent experiments. ANOVA followed by Bonferroni, $*P < 0.05$, $**P < 0.01$, $***P < 0.001$ versus untreated, $\#P < 0.05$, $###P < 0.001$ versus INSIE-ctr cells treated in the same way.

large LDs in cell clones exposed to FFA (Fig. 8D and E). Former studies proposed that the expression pattern of specific Plin proteins like lipid composition might be involved in the regulation of LD size (42). The presence of small LDs has been shown to correlate with increased lipotoxicity in various cell types, while large LDs enable an efficient storage of cellular lipids (40, 61, 62). In line with the expression profile of LD proteins, untreated INSIE-ctr cells displayed around 60% LDs of very small/small size and 40% of medium/large size (Fig. 8D). While this proportion was not significantly changed upon exposure to PA, OA exposure resulted in accelerated formation of large LDs (Fig. 8D and E). In contrast, INSIE-SPL cells exhibited an increase of very small LDs upon exposure to PA and also to OA (Fig. 8D and E). Interestingly, INSIE-SGPP1 cells were rich in medium size LDs under basal conditions, and the number of very small LDs was significantly decreased in OA-treated cells (Fig. 8D). Additionally, we observed the presence of large LDs in PA and even more in OA-treated INSIE-SGPP1 cells (Fig. 8D and E).

We extended these observations by employing the LipidTox combined with the LysoTracker staining, to establish whether LD removal by lysosomes could also be causative for the lower LD number observed in INSIE-SPL cells. The LipidTox staining allows the detection of neutral lipid accumulation in cells and has an extremely high affinity for neutral lipid droplets. Using this method, we observed a diffused neutral lipid staining, with a mild colocalization with lysosomes, in untreated INSIE-ctr and INSIE-SPL cells (Fig. 8F). In untreated INSIE-SGPP1 cells, the lipid staining was less diffuse, and well-defined LDs were detected (Fig. 8F). Following PA incubation, we noticed a more intense staining of lipids with a minimal LD presence and spatial distribution of lysosomes in INSIE-ctr cells. In contrast, a strong correlation of lipid and lysosome staining was visible in PA-treated INSIE-SPL cells, however, without LD-like structures and a high condensation of lysosomal network, suggesting activation of the lysosomal stress response (Fig. 8F). The incubation with PA did not increase the cytosolic lipid staining, but instead led to LD formation in INSIE-SGPP1 cells (Fig. 8F). In OA-treated INSIE-ctr cells, we observed a predominant LD presence and a weak overall and diffused lipid staining. Around 50% of LDs colocalized with lysosomes, indicating their functional turnover and an intact lysosomal network. The distribution of LipidTox staining in OA-treated INSIE-SPL cells was different; only a minor number of LDs, mainly of a smaller size, together with a diffused staining of the cytoplasmic compartment were evident (Fig. 8F). These small LDs colocalized with the lysosomal marker, indicating a high activity of lipophagy (Fig. 8F). In INSIE-SGPP1 cells, OA treatment increased the number of LDs, and many large LDs were distinguished (Fig. 8F). In contrast to INSIE-ctr and INSIE-SPL cells, the colocalization with the lysosomal tracker was rather

scarce, indicating a lower rate of lipophagy (Fig. 8F). Apparently, SGPP1 overexpression improves lipid storage capacity in INSIE cells, whereas the opposite is true for SPL overexpression.

Since we detected ceramide accumulation in mitochondria along with impaired mitochondrial functions in FFA-treated INSIE-SPL cells, we performed a double-immunostaining of mitochondria with Plin5, an LD protein that has been shown to be involved in LD-mitochondria interaction and lipid transfer into mitochondria (supplemental Fig. S2). We observed Plin5 staining with spherical structures of various sizes that sometimes colocalized with mitochondria (supplemental Fig. S2). In PA-treated INSIE-ctr cells, the presence of Plin5-mitochondria costaining was detected (supplemental Fig. S2). In OA-treated INSIE-ctr cells, a large number of Plin5-LD structures was visible, but only a minority of small size LD-Plin5 structures colocalized with mitochondria (supplemental Fig. S2). In INSIE-SPL cells, a lower number of Plin5-LD structures was detected, in line with a lower Plin5 expression, but an increased co-staining of Plin5 and mitochondria was observed after exposure to PA as well as to OA (supplemental Fig. S2). In INSIE-SGPP1 cells, most of the Plin5-LDs did not colocalize with mitochondria (supplemental Fig. S2). Note that colocalization of Plin5 and mitochondria was specific, while the double immunofluorescence staining of Plin3 with mitochondria did not result in any colocalization (data not shown). These data are indicative of an increased lipid transfer from LDs to mitochondria in SPL overexpressing beta-cells that could cause an increased mitochondrial metabolism contributing to ROS formation. On the other hand, a decreased Plin5/mitochondria colocalization observed in INSIE-SGPP1 cells could be partially responsible for a lower ATP content, but a lack of oxidative stress in mitochondria in these cells.

To assess an impact of the observed lower capacity of lipid storage on the rate of lipid peroxidation, which is thought to correlate with PA toxicity in beta-cells (46), we performed a Bodipy 581/591 C11 staining (Fig. 8G). As expected, we observed a strong induction of lipid peroxidation in INSIE-ctr cells treated with PA, and no significant induction after exposure to OA (Fig. 8G). Surprisingly, both INSIE-SPL and INSIE-SGPP1 cells were protected against lipid peroxidation in response to FFA, with a slightly more efficient effect in SGPP1 overexpressing cells (Fig. 8G). Thus, an increased toxicity of FFA observed in INSIE-SPL cells did not depend on lipid peroxidation.

SIP turnover influences the sensitivity to FFA and lipid droplets formation in human EndoC- β H1 beta-cells

In the last step of our study, we verified our findings from rat INSIE cells in the well-characterized human EndoC- β H1 beta-cells, which share a very similar

glucose responsiveness and sensitivity to FFA with human islets (7, 28). Interestingly, the expression of SPL, but not of SGPP1, is significantly higher in EndoC- β H1 beta-cells as compared to INSIE cells (Fig. 9). For this reason, we modified the expression of SPL (siRNA-mediated suppression) and of SGPP1 (lentiviral-mediated overexpression) and analyzed the sensitivity to FFA (Fig. 9C). In line with former studies (5–8), we observed significantly induced caspase-3/7 activation in response to PA as well as to OA in control EndoC- β H1 beta-cells, which was counteracted by SPL suppression (Fig. 9A). Interestingly, SGPP1 overexpression resulted in a significant reduction of PA-mediated caspase-3/7 activation but did not provide any protection against OA (Fig. 9A). Knockdown of SPL in SGPP1-overexpressing EndoC- β H1 beta-cells shut down the PA-related induction of apoptosis completely; however, did not prevent OA-mediated toxicity (Fig. 9A). Indeed, OA seemed to be slightly more toxic after SPL suppression than in EndoC- β H1-SGPP1 beta-cells with an abundant SPL expression.

Next, we analyzed the OA-mediated LD formation in EndoC- β H1 beta-cells with a genetically modified expression of SPL and/or SGPP1 (Fig. 9B). In line with earlier studies, we observed an increased LD formation in response to OA in control EndoC- β H1 beta-cells (Fig. 9B), which was enhanced after SPL suppression (Fig. 9B). In EndoC- β H1-SGPP1 cells, the number and size of LD was higher than in control cells (Fig. 9B). In EndoC- β H1-SGPP1 beta-cells with a reduced SPL expression, we observed numerous and particularly big LD, which tended to form clusters that filled the cytoplasm (Fig. 9B). Thus, the results obtained in human beta-cells confirm the distinct role of SPL versus SGPP1 in LD formation, which was observed in rat beta-cells. The lack of a protective effect after exposure to OA in EndoC- β H1-SGPP1 beta-cells with SPL knockdown correlated with the presence of unusual big and numerous LDs. This phenomenon of building enormously big hubs of LDs in EndoC- β H1 beta-cells under a parallel SPL suppression and SGPP1 overexpression might be related to an abundant expression of SCD1, an enzyme which has been recently shown to control LD formation in beta-cells (7, 40).

DISCUSSION

Disturbances of lipid metabolism and storage capacity have been suggested to contribute to lipotoxic beta-cell failure, but the underlying molecular mechanisms are still unclear. Interestingly, our study shows that the well-described effects of FFA (2, 5, 8–11) are differentially affected by the stimulation of SIP turnover; yet in an opposite way: with proapoptotic effects of SPL and protection provided by SGPP1 overexpression. Apparently, the metabolic fate of SIP and the subcellular compartment in which SIP is metabolized determine

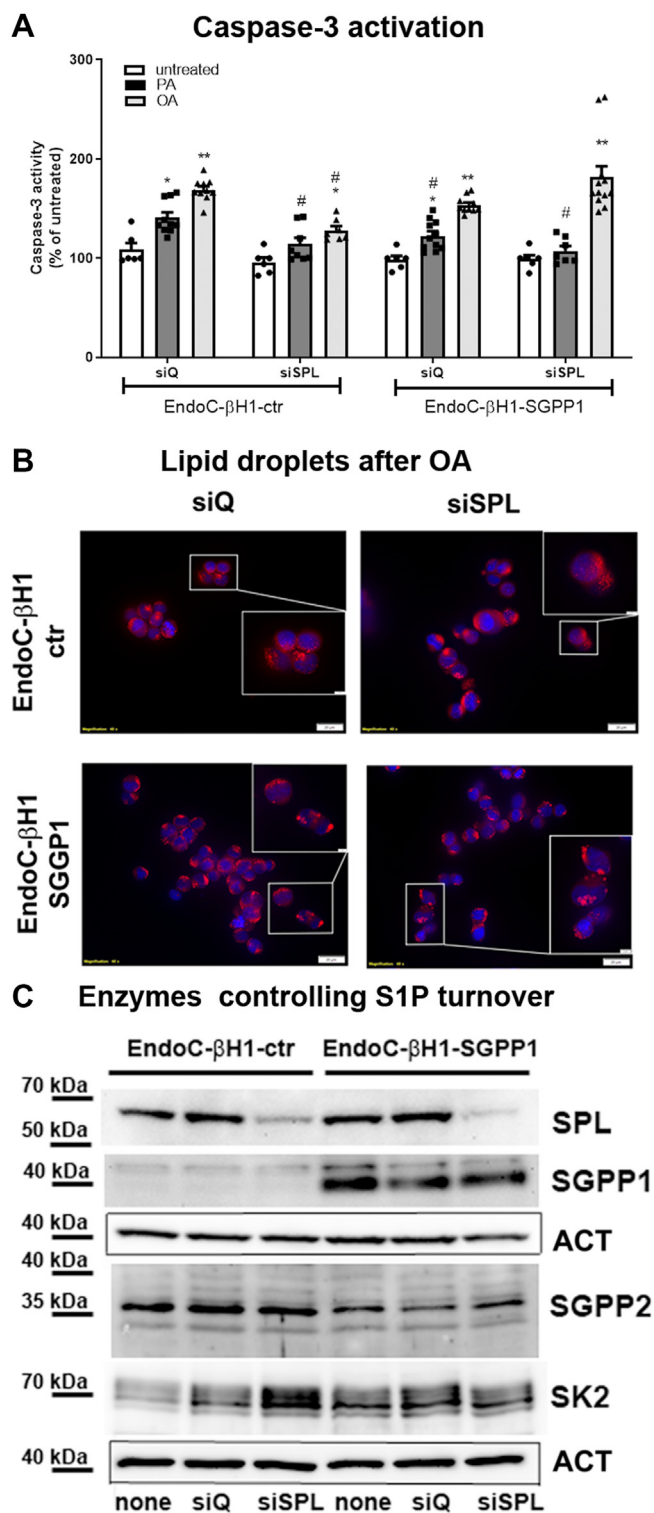


Fig. 9. Effects of SIP turnover and free fatty acids on caspase-3/7 activation and lipid droplet formation in human EndoC- β H1 beta-cells. EndoC- β H1 beta-cells were incubated in the absence or presence of PA or OA (500 μ M of each) for 24 h. Shown are (A) caspase-3/7 activation measured by Caspase-3/7-Glo assay (MEANS \pm SEM from $n = 6-10$), (B) lipid droplet formation visualized by OilRed staining (representative pictures from $n = 3$), (C) representative Western blots for the detection of SPL, SGPP1, SGPP2, and SK2 from 3–4 independent experiments. ANOVA followed by Bonferroni, * $P < 0.05$, ** $P < 0.01$, versus untreated, # $P < 0.05$, versus INSIE-ctr cells treated in the same way. Bars: 20 μ m, inset bars: 2 μ m.

whether a FFA exerts a toxic versus protective effect on beta-cells.

To uncover the mechanisms underlying these differential effects of SPL versus SGPP1, we analyzed in detail molecular pathways typically involved in lipotoxic beta-cell death. Our former study suggested that SPL overexpression might accelerate overall oxidative stress (8). We now further characterized the effects of two different paths of SIP metabolism on the generation of H₂O₂ in various cellular organelles. Our results demonstrate that overexpression of SPL but not of SGPP1 leads to an elevated FFA-induced H₂O₂ formation not only in peroxisomes, as typical H₂O₂ sources under lipotoxic stress in beta-cells (52, 63), but also in the cytosol and in mitochondria. Consistently, a higher expression of CuZnSOD (Tang, unpublished) and of MnSOD superoxide dismutases responsible for a higher capacity of H₂O₂ generation in the cytosol and in mitochondria, respectively, was identified. The increased SOD expression could additionally enhance the well-known imbalance of H₂O₂ formation and detoxification in beta-cells (48). In addition, the induction of mitochondrial H₂O₂ in PA- and—to a lesser extent—in OA-treated INSIE-SPL cells coincided with a significantly higher expression of CerS6, increased generation of Cer 14:0, Cer 16:0, and Cer 20:0, and mitochondrial ceramide accumulation as compared to INSIE-ctr cells. Former studies have demonstrated ceramide-induced oxidative stress in mitochondria and induction of apoptosis in other cell types (55, 64). Moreover, as reported for other cell types (65), elevation of H₂O₂ and of ceramide generation in FFA-treated INSIE-SPL cells correlated with profound mitochondrial fragmentation and hence with a drop of ATP content. Accordingly, CerS6-derived ceramides have been shown recently to interact with the mitochondrial fission factor to boost mitochondrial fragmentation in obesity (66) and to induce mitochondrial dysfunction and apoptosis in beta-cells (19, 27, 29). The vicious cycle leading to mitochondrial failure in FFA-treated INSIE-SPL cells was potentiated by a significantly lower expression of Cert1 paralleled by an increased expression of neutral sphingomyelinase and of SGPP2, thus impeding on the one hand ceramide transport to the Golgi and on the other hand providing more sphingosine, the substrate for efficient ceramide formation. An increased expression of neutral sphingomyelinase has been shown before to lead to ceramide generation in ER and mitochondria in INSIE beta-cells via an iPLA(2)beta-dependent pathway (67). Additionally, the observed deleterious effects of SPL overexpression on mitochondrial integrity could be also related to the reaction product of SPL, 2-hexadecenal, which has been shown to induce mitochondrial damage in other cell models (68). However, in line with the abundant expression of Aldh3a2 in INSIE-SPL cells, we were unable to detect hexadecenal by mass-spec, an observation which suggests its rapid metabolism and

argues against its involvement in the observed higher toxicity of FFA in these cells. In contrast to INSIE-SPL cells, the mitochondrial network remained intact in INSIE-SGPP1 cells exposed to FFA, with a rich network of elongated mitochondria with a higher activity of mitochondrial fusion mechanisms. Moreover, unlike in INSIE-ctr and SPL overexpressing cells, the expression of Lonpl was not stimulated upon FFA incubation, strengthening the notion that mitochondria of INSIE-SGPP1 cells were protected from FFA-mediated damage. Consistently, mitochondrial ceramide levels were significantly lower in these cells in which FFA treatment failed to stimulate CerS6 expression, while not affecting Cert1 expression. To the best of our knowledge, this is the first report visualizing mitochondrial ceramide distribution in beta-cells exposed to FFA and demonstrating the effects of SIP turnover pathways on mitochondrial integrity and ATP content in beta-cells.

In beta-cells, ceramide overload has also been associated with FFA-induced ER and oxidative stress (2, 19, 27–30, 69). In the present study, we demonstrated that these deleterious events strongly depended on the irreversible degradation of SIP, but not on SIP as a starting point of the recycling pathway catalyzed by SGPP1. The SGPP1-mediated protective effects went along with a considerable inhibition especially of the rate-limiting step of the de novo sphingolipid biosynthesis. Moreover, the expression of CerS5, which produces proapoptotic C16 ceramide, was significantly lower in INSIE-SGPP1 cells as compared to INSIE-ctr and SPL-overexpressing cells. On the other hand, CerS2, which generates beta-cell protective ceramides (C-length >24) (70), was increased by FFA in INSIE-SGPP1 cells in a similar manner as in INSIE-ctr cells. Quantitative measurements revealed, however, that the main difference between FFA-treated cell clones was in the content of short-chain ceramides that are well known for their proapoptotic effects. Importantly, OA diminished the formation of such ceramides in INSIE-ctr cells in contrast to INSIE-SPL cells. Although many different ceramide species could be detected at low levels in INSIE-SGPP1 cells, the most abundant ceramide species in these cells was Cer 24:0 and Cer 24:1. This was in line with an abundant expression of Ormdl3 and lower amounts of SPTlc. Unlikely as in INSIE-SPL cells, where Cert1 protein expression was significantly lower than INSIE-ctr cells, in INSIE-SGPP1 cells, no reduction was observed and the basal expression of Cert1 indeed tended to be higher than the other cells studied. Altogether, this data suggest a shift of ceramide generation from proapoptotic short chain to long chain ceramide species and a dramatic transfer of these ceramides from the ER to the Golgi and to the plasma membrane or other cellular structures/organelles (e.g., lipid droplets), thereby preventing ceramide-mediated oxidative stress induction and damage of ER and mitochondria in INSIE-SGPP1 cells.

Former studies have shown that LDs can act as storage for different ceramide species and derivatives thereof (37). Accordingly, the number and size of LDs were both significantly enhanced in INSIE-SGPP1 cells as compared to control cells. In contrast, SPL overexpression blunted lipid storage capacity as shown by a reduced LD number and size. Accordingly, we observed a high number of LDs after suppression of SPL in OA-treated human EndoC- β HI beta-cells. This effect was further potentiated by SGPP1 overexpression and accompanied by the formation of particularly large LD hubs as discussed above. The underlying mechanism of these changes could involve LD biogenesis and/or lipophagy. Intriguingly, the expression of seipin, an ER protein necessary for LD biogenesis, was found to be significantly increased only by OA in INSIE-SGPP1 and in control cells suggesting that additional factors are required for the observed changes of LDs in beta-cells under the studied conditions. One might be the composition of cellular lipids, which has been recently reported to play an important role for the expression and recruitment of specific Plin proteins to LD mantle in INSIE cells with an altered SCD1 expression and activity (40). SCD1-dependent disturbances in LD enrichment were shown to impact beta-cell susceptibility to PA (40). In contrast to INSE-SPL cells that were characterized by a significantly lower expression of Plin2 and Plin5, a significantly higher expression of these two LD proteins was detected in INSIE-SGPP1 cells. Plin5 was shown to protect against oxidative stress and mitochondrial damage in HepG2 cells (71) and to facilitate islet FA mobilization (61). An additional mechanism that could participate in a higher LD biogenesis in INSIE-SGPP1 cells could rely on the inhibited Dgat2 expression in response to FFA. Indeed, in kidney organoids, DGAT1 inhibition reduced LD number, while DGAT2 inhibition increased LD content via APOL1 and was associated with a drop of cytotoxicity (72). LD number can be also regulated by lipophagy, an autophagic pathway ending up by lysosomal degradation of LDs (73). The released neutral lipids are available for energy production and other reactions, which might lead to utilization of FA for the generation of bioactive lipids. A properly controlled lipophagy is believed to participate in the maintenance of cellular metabolism, while protecting from lipotoxicity (38). Therefore, INSIE-SGPP1 cells that were characterized by a blunted lipophagy could be more efficiently protected against lipotoxicity, but in turn obtain less fuel for ATP production. This was in contrast to a hyperactivated lipophagy, as observed in INSIE-SPL cells, which could result in undesired oversupply of FA for further metabolism and β -oxidation contributing to the induction of oxidative stress under FFA exposure. The hyperactive lipophagy in INSIE-SPL cells could be supported by a higher content of phosphatidylethanolamine, generated from phosphoethanolamine, a reaction product of SPL (44). Note that PE is recruiting

and anchoring LC3 to autophagosomal membranes, an essential step for their formation and processing.

Intriguingly, the distinct effects of SPL and SGPP1 were largely related to oxidative stress but independent of FFA-mediated lipid peroxidation. PA, but not OA, induced lipid peroxidation in INSIE-ctr cells, that was significantly blunted by overexpression of both, SPL and SGPP1. It has been recently reported that H_2O_2 generated in peroxisomes, ER, and mitochondria during metabolic processes of FFA, and redox reactions is required for the membrane lipid peroxidation in INSIE beta-cells (46). In our study, SGPP1 overexpression inhibited FFA-induced H_2O_2 generation in the cytoplasm, peroxisomes, and mitochondria. This obviously constitutes a protective mechanism to prevent PA-induced lipid peroxidation. On the other hand, in INSIE-SPL cells, a considerable upregulation of H_2O_2 generation in various cellular compartments was also accompanied by a significant reduction of lipid peroxidation. A possible explanation of this paradoxical effect could be the fact that SPL represents a branching point of sphingolipid and glycerophospholipid metabolism, and changes of its activity were shown to largely affect membrane lipid composition (34). Thus, SPL overexpression might cause a change of the PUFA/MUFA ratio in membrane lipids in favor of MUFAs, known to prevent lipid peroxidation, as recently reported in OA-treated INSIE cells (46). Additionally, the lack of lipid peroxidation in SPL overexpressing cells emphasizes an essential role of proapoptotic ceramide generation particularly at the mitochondria/ER contact sides and its accumulation due to the lack of a proper lipid storage capacity for lipotoxicity in beta-cells.

Further investigations are needed to uncover the mechanisms involved in the observed changes regarding the expression of various sphingolipid metabolic enzymes as well as of mitochondrial and LD proteins. These changes may be related to the reported epigenetic regulation by SIP (74, 75), particularly in the case of INSIE-SPL cells, which display a considerably reduced SIP content. Although SIP concentration was also significantly reduced in INSIE-SGPP1 cells, the effect was less pronounced due to a parallel upregulation of SK2 and downregulation of SGPP2. Therefore, one would not expect a considerable effect on epigenetic regulation, especially in the case of genes subjected to more complex transcriptional regulatory mechanisms. However, changes of the lipidome as a result of SPL or SGPP1 overexpression might also affect the regulation of gene transcription via altered lipid signaling pathways.

Finally, by validating our findings in human beta-cells, we confirmed the concept of distinct effects of SPL versus SGPP1 on FFA toxicity and LD formation. Thus, our study clearly shows that enzymes involved in SIP turnover are crucial for lipotoxic stress in beta-cells (summarized in Fig. 10). Our study also demonstrates that the sensitivity of beta-cells to FFA is not solely

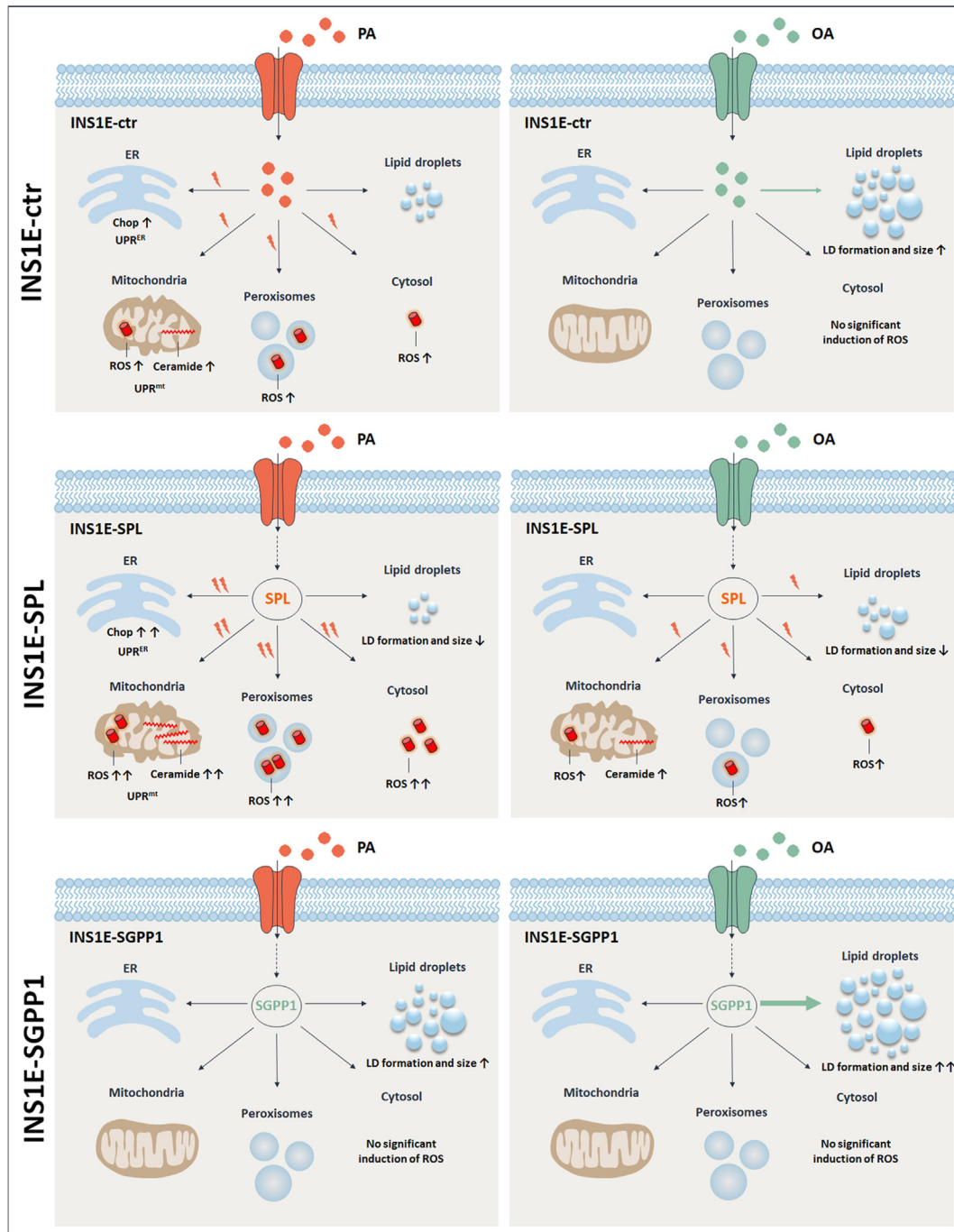



Fig. 10. Schematic summary of the differential effects of SPL versus SGPP1 on FFA-mediated toxicity in pancreatic beta-cells. In INS1E-ctr cells, PA induces ER stress, mild mitochondrial stress related to the accumulation of proapoptotic ceramides in mitochondria and oxidative stress (H_2O_2 formation mainly in cytoplasm and peroxisomes), while OA is not toxic and stimulates lipid droplets formation. The enhanced SIP cleavage capacity by SPL overexpression accelerates toxic effects of PA and sensitized to OA via potentiation of oxidative and ER stress responses as well as reduction of lipid storage capacity accompanied by a massive accumulation of pro-apoptotic ceramides in mitochondria. SGPP1 overexpression protects against lipotoxicity via upregulation of lipid storage (LD particularly of a bigger size) and decrease in ceramide formation. For details with regard to human beta cells, look in Discussion. ER, endoplasmic reticulum, LD, lipid droplet, ROS, reactive oxygen species, UPR^{ER} , ER unfolded protein response, UPR^{mt} , mitochondrial unfolded protein response.

regulated by the intracellular SIP concentration per se but also by the metabolic pathway to which SIP is subjected and the subcellular compartments affected. Further studies are needed to investigate how the observed effects of intracellular SIP turnover in beta-

cells might influence their sensitivity to FFA in a complex islet environment, with additional inputs of SIP and/or other bioactive metabolites produced and secreted from other islet cell types as well as exocrine tissue or islet vascular and innervation systems.

Overall, the results of the present study open new perspectives regarding the contribution of SIP turnover in beta-cells affected in T2DM patients. Hence, therapeutic strategies aiming on a specific and tight regulation of intracellular SIP turnover may turn out as an attractive tool for future pharmacological protection of beta-cell function in T2DM.

Data availability

All relevant data for this study are included in this manuscript. The data which were not shown are available upon request from the corresponding author. 

Supplemental data

This article contains [supplemental data](#).


Acknowledgments

This is a part of Y. T. doctoral thesis project. We thank Dr Matthias Elsner (Institute of Clinical Biochemistry, Hannover Medical School, Hannover, Germany) for the pLenti-HyPer-Peroxi vector and INSIE-ctr-HyPer-Peroxi beta-cells.

Author contributions

Y. T., M. M., P. W., and Bo. L. formal analysis; Y. T., M. M., Br. L., I. M., P. W., N. S., and E. G.-C. investigation; Y. T., Br. L., I. M., P. W., and Bo. L. methodology; Y. T. and E. G.-C. visualization; Y. T. and E. G.-C. writing—original draft; M. M., P. W., J. D. S., G. v. E. D., and E. G.-C. writing—review and editing; J. D. S. resources; G. v. E.-D. and E. G.-C. validation; E. G.-C. conceptualization; J. D. S., G. v. E. D., and E. G.-C. data curation; E. G.-C. funding acquisition; E. G.-C. project administration; E. G.-C. supervision.

Author ORCIDs

Iilir Mehmeti  <https://orcid.org/0000-0003-1923-0837>
Bodo Levkau  <https://orcid.org/0000-0002-0005-125X>
Gerhild van Echten-Deckert  <https://orcid.org/0000-0002-2816-7852>
Ewa Gurgul-Convey  <https://orcid.org/0000-0002-9269-266X>

Funding and additional information

This research was funded by German Research Foundation – project number 521990259 to E. G.-C. Y. T. was supported by the CSC scholarship.

Conflict of interest

The authors declare that they have no conflicts of interests with the contents of this article.

Abbreviations

Aldh3a2, aldehyde dehydrogenase 3 family member A2; APOL1, apolipoprotein L1; CD, ceramidase; Cer, ceramide; CerS, ceramide synthase; Cert1, ceramide transporter 1; Chop, C/EBP homologous protein; CuZnSOD, copper/zinc superoxide dismutase; DAPI, 4,6-diamidino-2-phenylindole; DCFDA, dichlorodihydrofluorescein diacetate; Degs, dihydroceramide desaturase 1; ER, endoplasmic reticulum; LC3, microtubule associated protein 1 light chain 3; LD, lipid droplets; Lonpl, mitochondrial Lon protease-like protein;

MnSOD, manganese superoxide dismutase; MTT, 3-(4,5-dimethylthiazol-2-yl)-2,5-diphenyl tetrazolium bromide; MUFA, monounsaturated fatty acids; OA, oleate; ORMDL3, orosomucoid like-3 (ORMDL sphingolipid biosynthesis regulator) 3; PA, palmitate; PE, phosphatidylethanolamine; Plin, perilipin; Phb2, prohibitin 2; PUFA, polyunsaturated fatty acids; ROS, reactive oxygen species; SCD1, stearoyl-CoA desaturase-1; SGPPI, SIP phosphatase 1; SK1/2, sphingosine kinase 1/2; SM, sphingomyelin; SIP, sphingosine 1 phosphate; SPL, SIP lyase; SPT, serine palmitoyl transferase; SPTlc, serine palmitoyl transferase long chain; T2DM, type 2 diabetes mellitus.

Manuscript received December 19, 2023, and in revised form June 7, 2024. Published, JLR Papers in Press, June 29, 2024, <https://doi.org/10.1016/j.jlr.2024.100587>

REFERENCES

1. Ahmad, E., Lim, S., Lamptey, R., Webb, D. R., and Davies, M. J. (2022) Type 2 diabetes. *Lancet*. **400**, 1803–1820
2. Lytrivi, M., Castell, A. L., Poutou, V., and Cnop, M. (2020) Recent insights into mechanisms of beta-cell lipo- and glucolipotoxicity in type 2 diabetes. *J. Mol. Biol.* **432**, 1514–1534
3. Franks, P. W., and Merino, J. (2018) Gene-lifestyle interplay in type 2 diabetes. *Curr. Opin. Genet. Dev.* **50**, 35–40
4. Takabe, K., Paugh, S. W., Milstien, S., and Spiegel, S. (2008) "Inside-out" signaling of sphingosine-1-phosphate: therapeutic targets. *Pharmacol. Rev.* **60**, 181–195
5. Plötz, T., von Hanstein, A. S., Krümmel, B., Laporte, A., Mehmeti, I., and Lenzen, S. (2019) Structure-toxicity relationships of saturated and unsaturated free fatty acids for elucidating the lipotoxic effects in human EndoC-betaHI beta-cells. *Biochim. Biophys. Acta Mol. Basis Dis.* **1865**, 165525
6. von Hanstein, A. S., Lenzen, S., and Plötz, T. (2020) Toxicity of fatty acid profiles of popular edible oils in human EndoC-betaHI beta-cells. *Nutr. Diabetes*. **10**, 5
7. von Hanstein, A. S., Tsikas, D., Lenzen, S., Jorns, A., and Plotz, T. (2023) Potentiation of lipotoxicity in human EndoC-betaHI beta-cells by glucose is dependent on the structure of free fatty acids. *Mol. Nutr. Food Res.* **67**, e2200582
8. Tang, Y., Plötz, T., Gräler, M. H., and Gurgul-Convey, E. (2021) Sphingosine-1 phosphate lyase regulates sensitivity of pancreatic beta-cells to lipotoxicity. *Int. J. Mol. Sci.* **22**, 10893
9. Gehrman, W., Wurdemann, W., Plötz, T., Jörns, A., Lenzen, S., and Elsner, M. (2015) Antagonism between saturated and unsaturated fatty acids in ROS mediated lipotoxicity in rat insulin-producing cells. *Cell Physiol. Biochem.* **36**, 852–865
10. Plötz, T., Krümmel, B., Laporte, A., Pingitore, A., Persaud, S. J., Jörns, A., et al. (2017) The monounsaturated fatty acid oleate is the major physiological toxic free fatty acid for human beta cells. *Nutr. Diabetes*. **7**, 305
11. Oshima, M., Pechberty, S., Bellini, L., Gopel, S. O., Campana, M., Rouch, C., et al. (2020) Stearoyl CoA desaturase is a gatekeeper that protects human beta cells against lipotoxicity and maintains their identity. *Diabetologia*. **63**, 395–409
12. Kowalski, G. M., Carey, A. L., Selathurai, A., Kingwell, B. A., and Bruce, C. R. (2013) Plasma sphingosine-1-phosphate is elevated in obesity. *PLoS One*. **8**, e72449
13. Tanaka, S., Kanazawa, I., and Sugimoto, T. (2018) Visceral fat accumulation is associated with increased plasma sphingosine-1-phosphate levels in type 2 diabetes mellitus. *Diabetes Res. Clin. Pract.* **143**, 146–150
14. Fayyaz, S., Japtok, L., and Kleuser, B. (2014) Divergent role of sphingosine 1-phosphate on insulin resistance. *Cell Physiol. Biochem.* **34**, 134–147
15. Hannun, Y. A., and Obeid, L. M. (2018) Sphingolipids and their metabolism in physiology and disease. *Nat. Rev. Mol. Cell Biol.* **19**, 175–191
16. Quehenberger, O., Armando, A. M., Brown, A. H., Milne, S. B., Myers, D. S., Merrill, A. H., et al. (2010) Lipidomics reveals a remarkable diversity of lipids in human plasma. *J. Lipid Res.* **51**, 3299–3305

17. Hahn, C., Tyka, K., Saba, J. D., Lenzen, S., and Gurgul-Convey, E. (2017) Overexpression of sphingosine-1-phosphate lyase protects insulin-secreting cells against cytokine toxicity. *J. Biol. Chem.* **292**, 20292–20304
18. Cantrell Stanford, J., Morris, A. J., Sunkara, M., Popa, G. J., Larson, K. L., and Ozcan, S. (2012) Sphingosine 1-phosphate (S1P) regulates glucose-stimulated insulin secretion in pancreatic beta cells. *J. Biol. Chem.* **287**, 13457–13464
19. Veret, J., Coant, N., Gorshkova, I. A., Giussani, P., Fradet, M., Riccielli, E., *et al.* (2013) Role of palmitate-induced sphingoid base-1-phosphate biosynthesis in INS-1 beta-cell survival. *Biochim. Biophys. Acta* **1831**, 251–262
20. Qi, Y., Chen, J., Lay, A., Don, A., Vadas, M., and Xia, P. (2013) Loss of sphingosine kinase 1 predisposes to the onset of diabetes via promoting pancreatic beta-cell death in diet-induced obese mice. *FASEB J.* **27**, 4294–4304
21. Ravichandran, S., Finlin, B. S., Kern, P. A., and Ozcan, S. (2019) Sphk2(-/-) mice are protected from obesity and insulin resistance. *Biochim. Biophys. Acta Mol. Basis Dis.* **1865**, 570–576
22. Song, Z., Wang, W., Li, N., Yan, S., Rong, K., Lan, T., *et al.* (2019) Sphingosine kinase 2 promotes lipotoxicity in pancreatic beta-cells and the progression of diabetes. *FASEB J.* **33**, 3636–3646
23. Maceyka, M., Sankala, H., Hait, N. C., Le Stunff, H., Liu, H., Toman, R., *et al.* (2005) SphK1 and SphK2, sphingosine kinase isoenzymes with opposing functions in sphingolipid metabolism. *J. Biol. Chem.* **280**, 37118–37129
24. Gurgul-Convey, E. (2022) To be or not to be: the divergent action and metabolism of sphingosine-1 phosphate in pancreatic beta-cells in response to cytokines and fatty acids. *Int. J. Mol. Sci.* **23**, 1638
25. Maceyka, M., Milstien, S., and Spiegel, S. (2009) Sphingosine-1-phosphate: the Swiss army knife of sphingolipid signaling. *J. Lipid Res.* **50** (Suppl), S272–S276
26. Aguilar, A., and Saba, J. D. (2012) Truth and consequences of sphingosine-1-phosphate lyase. *Adv. Biol. Regul.* **52**, 17–30
27. Gjoni, E., Brioschi, L., Cinque, A., Coant, N., Islam, M. N., Ng, C. K., *et al.* (2014) Glucolipotoxicity impairs ceramide flow from the endoplasmic reticulum to the Golgi apparatus in INS-1 beta-cells. *PLoS One* **9**, e110875
28. Lupi, R., Dotta, F., Marselli, L., Del Guerra, S., Masini, M., Santangelo, C., *et al.* (2002) Prolonged exposure to free fatty acids has cytostatic and pro-apoptotic effects on human pancreatic islets: evidence that beta-cell death is caspase mediated, partially dependent on ceramide pathway, and Bcl-2 regulated. *Diabetes* **51**, 1437–1442
29. Veret, J., Coant, N., Berdyshev, E. V., Skobeleva, A., Therville, N., Bailbe, D., *et al.* Gorshkova, I., Natarajan, V., Portha, B., and Le Stunff, H. (2011) Ceramide synthase 4 and de novo production of ceramides with specific N-acyl chain lengths are involved in glucolipotoxicity-induced apoptosis of INS-1 beta-cells. *Biochem. J.* **438**, 177–189
30. Boslem, E., Weir, J. M., MacIntosh, G., Sue, N., Cantley, J., Meikle, P. J., *et al.* (2013) Alteration of endoplasmic reticulum lipid rafts contributes to lipotoxicity in pancreatic beta-cells. *J. Biol. Chem.* **288**, 26569–26582
31. Kunkel, G. T., Maceyka, M., Milstien, S., and Spiegel, S. (2013) Targeting the sphingosine-1-phosphate axis in cancer, inflammation and beyond. *Nat. Rev. Drug Discov.* **12**, 688–702
32. Taguchi, Y., Allende, M. L., Mizukami, H., Cook, E. K., Gavrilova, O., Tuymetova, G., *et al.* (2016) Sphingosine-1-phosphate phosphatase 2 regulates pancreatic islet beta-cell endoplasmic reticulum stress and proliferation. *J. Biol. Chem.* **291**, 12029–12038
33. Deevska, G. M., and Nikolova-Karakashian, M. N. (2017) The expanding role of sphingolipids in lipid droplet biogenesis. *Biochim. Biophys. Acta Mol. Cell Biol. Lipids* **1862**, 1155–1165
34. Bektas, M., Allende, M. L., Lee, B. G., Chen, W., Amar, M. J., Remaley, A. T., *et al.* (2010) Sphingosine 1-phosphate lyase deficiency disrupts lipid homeostasis in liver. *J. Biol. Chem.* **285**, 10880–10889
35. Zadoorian, A., Du, X., and Yang, H. (2023) Lipid droplet biogenesis and functions in health and disease. *Nat. Rev. Endocrinol.* **19**, 443–459
36. Itabe, H., Yamaguchi, T., Nimura, S., and Sasabe, N. (2017) Perilipins: a diversity of intracellular lipid droplet proteins. *Lipids Health Dis.* **16**, 83
37. Senkal, C. E., Salama, M. F., Snider, A. J., Allopenna, J. J., Rana, N. A., Koller, A., *et al.* (2017) Ceramide is metabolized to acylceramide and stored in lipid droplets. *Cell Metab.* **25**, 686–697
38. Geltinger, F., Tevini, J., Briza, P., Geiser, A., Bischof, J., Richter, K., *et al.* (2020) The transfer of specific mitochondrial lipids and proteins to lipid droplets contributes to proteostasis upon stress and aging in the eukaryotic model system *Saccharomyces cerevisiae*. *GeroScience* **42**, 19–38
39. Plötz, T., Hartmann, M., Lenzen, S., and Elsner, M. (2016) The role of lipid droplet formation in the protection of unsaturated fatty acids against palmitic acid induced lipotoxicity to rat insulin-producing cells. *Nutr. Metab.* **13**, 16
40. Janikiewicz, J., Dobosz, A. M., Majzner, K., Bernas, T., and Dobrzyn, A. (2023) Stearoyl-CoA desaturase 1 deficiency exacerbates palmitate-induced lipotoxicity by the formation of small lipid droplets in pancreatic beta-cells. *Biochim. Biophys. Acta Mol. Basis Dis.* **1869**, 166711
41. Kleinfeld, A. M., Prothro, D., Brown, D. L., Davis, R. C., Richieri, G. V., and DeMaria, A. (1996) Increases in serum unbound free fatty acid levels following coronary angioplasty. *Am. J. Cardiol.* **78**, 1350–1354
42. Cnop, M., Hannaert, J. C., Hoorens, A., Eizirik, D. L., and Pipeleers, D. G. (2001) Inverse relationship between cytotoxicity of free fatty acids in pancreatic islet cells and cellular triglyceride accumulation. *Diabetes* **50**, 1771–1777
43. Richieri, G. V., and Kleinfeld, A. M. (1995) Unbound free fatty acid levels in human serum. *J. Lipid Res.* **36**, 229–240
44. Spiller, S., Blüher, M., and Hoffmann, R. (2018) Plasma levels of free fatty acids correlate with type 2 diabetes mellitus. *Diabetes Obes. Metab.* **20**, 2661–2669
45. Hanzelka, K., Skalniak, L., Jura, J., Lenzen, S., and Gurgul-Convey, E. (2012) Effects of the novel mitochondrial protein mimitin in insulin-secreting cells. *Biochem. J.* **445**, 349–359
46. Krümmel, B., von Hanstein, A. S., Plötz, T., Lenzen, S., and Mehmeti, I. (2022) Differential effects of saturated and unsaturated free fatty acids on ferroptosis in rat beta-cells. *J. Nutr. Biochem.* **106**, 109013
47. Thomas, N., Schroder, N. H., Nowak, M. K., Wollnitzke, P., Ghaderi, S., von Wnuck Lipinski, K., *et al.* (2023) Sphingosine-1-phosphate suppresses GLUT activity through PP2A and counteracts hyperglycemia in diabetic red blood cells. *Nat. Commun.* **14**, 8329
48. Siow, D. L., Anderson, C. D., Berdyshev, E. V., Skobeleva, A., Pitson, S. M., and Wattenberg, B. W. (2010) Intracellular localization of sphingosine kinase 1 alters access to substrate pools but does not affect the degradative fate of sphingosine-1-phosphate. *J. Lipid Res.* **51**, 2546–2559
49. Mitroi, D. N., Karunakaran, I., Gräler, M., Saba, J. D., Ehninger, D., Ledesma, M. D., *et al.* (2017) SGPL1 (sphingosine phosphate lyase 1) modulates neuronal autophagy via phosphatidylethanolamine production. *Autophagy* **13**, 885–899
50. Wang, S., Robinet, P., Smith, J. D., and Gulshan, K. (2015) ORMDL orosomucoid-like proteins are degraded by free-cholesterol-loading-induced autophagy. *Proc. Natl. Acad. Sci. U. S. A.* **112**, 3728–3733
51. Cunha, D. A., Hekerman, P., Ladriere, L., Bazarra-Castro, A., Ortis, F., Wakeham, M. C., *et al.* (2008) Initiation and execution of lipotoxic ER stress in pancreatic beta-cells. *J. Cell Sci.* **121**, 2308–2318
52. Elsner, M., Gehrman, W., and Lenzen, S. (2011) Peroxisome-generated hydrogen peroxide as important mediator of lipotoxicity in insulin-producing cells. *Diabetes* **60**, 200–208
53. Mehmeti, I., Lortz, S., Avezov, E., Jörns, A., and Lenzen, S. (2017) ER-resident antioxidative GPx7 and GPx8 enzyme isoforms protect insulin-secreting INS-1E beta-cells against lipotoxicity by improving the ER antioxidative capacity. *Free Radic. Biol. Med.* **112**, 121–130
54. Lenzen, S. (2017) Chemistry and biology of reactive species with special reference to the antioxidative defence status in pancreatic beta-cells. *Biochim. Biophys. Acta Gen. Subj.* **1861**, 1929–1942
55. Siskind, L. J. (2005) Mitochondrial ceramide and the induction of apoptosis. *J. Bioenerg. Biomembr.* **37**, 143–153
56. Hanada, K., Kumagai, K., Yasuda, S., Miura, Y., Kawano, M., Fukasawa, M., *et al.* (2003) Molecular machinery for non-vesicular trafficking of ceramide. *Nature* **426**, 803–809
57. Tuuf, J., Kjellberg, M. A., Molotkovsky, J. G., Hanada, K., and Mattjus, P. (2011) The intermembrane ceramide transport catalyzed by CERT is sensitive to the lipid environment. *Biochim. Biophys. Acta* **1808**, 229–235

58. Salo, V. T., Li, S., Vihinen, H., Holtta-Vuori, M., Szkalitsy, A., Horvath, P., *et al* Belevich, L., Peranen, J., Thiele, C., Somerharju, P., Zhao, H., Santinho, A., Thiam, A. R., Jokitalo, E., and Ikonen, E. (2019) Seipin facilitates triglyceride flow to lipid droplet and counteracts droplet ripening via endoplasmic reticulum contact. *Dev. Cell.* **50**, 478–493.e9
59. Cartwright, B. R., and Goodman, J. M. (2012) Seipin: from human disease to molecular mechanism. *J. Lipid Res.* **53**, 1042–1055
60. McFie, P. J., Banman, S. L., and Stone, S. J. (2018) Diacylglycerol acyltransferase-2 contains a c-terminal sequence that interacts with lipid droplets. *Biochim. Biophys. Acta Mol. Cell Biol. Lipids.* **1863**, 1068–1081
61. Trevino, M. B., Machida, Y., Hallinger, D. R., Garcia, E., Christensen, A., Dutta, S., *et al* (2015) Perilipin 5 regulates islet lipid metabolism and insulin secretion in a cAMP-dependent manner: implication of its role in the postprandial insulin secretion. *Diabetes.* **64**, 1299–1310
62. Tong, X., Liu, S., Stein, R., and Imai, Y. (2022) Lipid droplets' role in the regulation of beta-cell function and beta-cell demise in type 2 diabetes. *Endocrinology.* **163**, bqac007
63. Gehrman, W., Elsner, M., and Lenzen, S. (2010) Role of metabolically generated reactive oxygen species for lipotoxicity in pancreatic beta-cells. *Diabetes. Obes. Metab.* **12** (Suppl 2), 149–158
64. Garcia-Ruiz, C., Colell, A., Mari, M., Morales, A., and Fernandez-Checa, J. C. (1997) Direct effect of ceramide on the mitochondrial electron transport chain leads to generation of reactive oxygen species. Role of mitochondrial glutathione. *J. Biol. Chem.* **272**, 11369–11377
65. Vaena, S., Chakraborty, P., Lee, H. G., Jannah, A. H., Kassir, M. F., Beeson, G., *et al* (2021) Aging-dependent mitochondrial dysfunction mediated by ceramide signaling inhibits antitumor T cell response. *Cell Rep.* **35**, 109076
66. Hammerschmidt, P., Ostkotte, D., Nolte, H., Gerl, M. J., Jais, A., Brunner, H. L., *et al* (2019) CerS6-Derived sphingolipids interact with Mff and promote mitochondrial fragmentation in obesity. *Cell.* **177**, 1536–1552.e23
67. Lei, X., Zhang, S., Bohrer, A., and Ramanadham, S. (2008) Calcium-independent phospholipase A2 (iPLA2 beta)-mediated ceramide generation plays a key role in the cross-talk between the endoplasmic reticulum (ER) and mitochondria during ER stress-induced insulin-secreting cell apoptosis. *J. Biol. Chem.* **283**, 34819–34832
68. Kumar, A., Byun, H. S., Bittman, R., and Saba, J. D. (2011) The sphingolipid degradation product trans-2-hexadecenal induces cytoskeletal reorganization and apoptosis in a JNK-dependent manner. *Cell. Signal.* **23**, 1144–1152
69. Epstein, S., Kirkpatrick, C. L., Castillon, G. A., Muniz, M., Riezman, I., David, F. P. A., *et al* (2012) Activation of the unfolded protein response pathway causes ceramide accumulation in yeast and INS-1E insulinoma cells. *J. lipid Res.* **53**, 412–420
70. Buschard, K., Fredman, P., Bog-Hansen, E., Blomqvist, M., Hedner, J., Rastam, L., *et al* (2005) Low serum concentration of sulfatide and presence of sulfated lactosylceramid are associated with Type 2 diabetes. The Skaraborg Project. *Diabet. Med.* **22**, 1190–1198
71. Tan, Y., Jin, Y., Wang, Q., Huang, J., Wu, X., and Ren, Z. (2019) Perilipin 5 protects against cellular oxidative stress by enhancing mitochondrial function in HepG2 cells. *Cells.* **8**, 1241
72. Chun, J., Riella, C. V., Chung, H., Shah, S. S., Wang, M., Magraner, J. M., *et al* (2022) DGAT2 inhibition potentiates lipid droplet formation to reduce cytotoxicity in APOL1 kidney risk variants. *J. Am. Soc. Nephrol.* **33**, 889–907
73. van Zutphen, T., Todde, V., de Boer, R., Kreim, M., Hofbauer, H. F., Wolinski, H., *et al* (2014) Lipid droplet autophagy in the yeast *Saccharomyces cerevisiae*. *Mol. Biol. Cell.* **25**, 290–301
74. Hait, N. C., Allegood, J., Maceyka, M., Strub, G. M., Harikumar, K. B., Singh, S. K., *et al* (2009) Regulation of histone acetylation in the nucleus by sphingosine-1-phosphate. *Science.* **325**, 1254–1257
75. Strub, G. M., Paillard, M., Liang, J., Gomez, L., Allegood, J. C., Hait, N. C., *et al* (2011) Sphingosine-1-phosphate produced by sphingosine kinase 2 in mitochondria interacts with prohibitin 2 to regulate complex IV assembly and respiration. *FASEB J.* **25**, 600–612